

Preprint Series

Space-Time Discretized Retarded Potential Boundary Integral Operators: Quadrature for Collocation Methods

Dominik Pölz, Martin Schanz

Institute of Applied Mechanics, Graz University of Technology

Accepted for publication in: *SIAM Journal on Scientific Computing*

Latest revision: October 7, 2019

Abstract

We propose a novel discretization method for time domain boundary integral equations of the 3d wave equation. The basic idea of the discussed approach is to treat time as if it were an additional spatial coordinate. This leads to a discretization of the boundary integral operators in 3+1 dimensional space-time by use of basis functions which do not separate space and time variables. These functions are based on tetrahedral meshes of the lateral boundary of the space-time cylinder. We discuss an explicit representation of the integral operators of the wave equation, so-called retarded potential integral operators, which genuinely conforms to the space-time setting. The majority of this work is concerned with the numerical evaluation of these integrals. An accurate and robust Gaussian quadrature scheme is proposed and verified by means of numerical experiments.

1 Introduction

The study of transient wave propagation processes plays a key role in various fields of modern engineering and applied sciences. In particular, the linear wave equation is a viable model for acoustic as well as electromagnetic waves in many situations. An important class of problems related to these types of waves are scattering problems, where the scattered wave field in the unbounded exterior of the scatterer is of interest. For such problems the boundary integral equation method is a promising approach, as it reduces the problem posed on the unbounded exterior to the bounded surface of the scatterer. Due to the strong Huygens principle the integral operators associated to the wave equation have a special structure, motivating the prominent term retarded potential boundary integral equations (RPBIEs).

The inherent advantages of RPBIEs inspired numerous publications dedicated towards their analysis and their discretization. The mathematical analysis of integral equations of hyperbolic problems was sparked by the seminal publications of Bamberger and Ha-Duong [4, 5]. Their approach uses the Laplace transform with respect to the time variable to transport results on the solution in Laplace domain to time domain. The review paper of Ha-Duong [34] and the book of Sayas [66] provide elegant overviews of this method. Rynne [59] and Sayas [65, 66] have developed time domain techniques based on the theory of hyperbolic equations and semigroups of operators respectively. The paper of Joly and Rodríguez [36] presents a thorough review and discussion of the existing literature and analyzes different bilinear forms of RPBIEs.

1.1 Boundary element methods for RPBIEs

Approximation techniques for RPBIEs can be traced back to Friedman and Shaw [22]. Mansur [47] developed the first boundary element method in the modern sense. The review article of Costabel and Sayas [12] and the preface in [66] present an excellent overview of the available literature. The following paragraphs attempt to provide a non-exhaustive overview of prominent boundary element methods for time domain integral equations.

As already mentioned, the first and perhaps most straightforward class of discretization schemes for RPBIEs has its origins in the work of Mansur [48, 47]. Within these procedures an ansatz for the unknown surface density is constructed as a product of separate ansatz functions in the space and time variable, see e.g. [11]. The RPBIE is collocated, i.e. interpolated, at certain collocation points on the spatial grid and at fixed time steps. Due to inherent stability issues of these schemes [10, 57, 60] several articles have been devoted towards their stabilization [58, 15, 14, 13].

A substantially more intricate approach is constituted by Galerkin methods based on space-time variational formulations of RPBIEs. The stability of these procedures is due to coercivity properties of certain bilinear forms associated to first kind RPBIEs [34]. Many papers were dedicated towards their development [30, 1, 61, 8, 71, 28, 29].

A distinguished discretization scheme goes back to Lubich's convolution quadrature method (CQM) [43, 44]. The convolution type time domain integral operators are approximated via the CQM, which is combined with standard spatial boundary element methods, e.g. collocation or Galerkin methods [45, 68, 7, 6, 3]. This approach has been extended to accommodate variable time step sizes in [40, 41, 42].

Moreover, there are boundary element methods for the wave equation that entirely avoid the

use of retarded potentials. In a variant of Rothe’s method [56] the initial-boundary value problem is discretized in time with a suitable implicit time-stepping scheme. The resulting stationary problem at each time step is solved by well-established boundary element methods for elliptic problems, see [12].

A common feature of virtually any yet implemented boundary element method for the wave equation is that they discretize space and time separately. In contrast, we seek to take a first step towards the development of a genuine space-time discretization method in this paper. The following paragraphs exhibit basic concepts and existing literature on the space-time methodology.

1.2 Space-time methodology

The basic idea of space-time methods is to treat the time variable as if it were an additional spatial coordinate. This thinking suggests to treat the transient problem as a single operator equation in space-time, even within the discretization. Consequently, one is confronted with a $d + 1$ dimensional computational domain, where $d \in \mathbb{N}$ is the number of spatial dimensions. This domain can be decomposed into finite elements in an unstructured fashion, i.e. without distinguishing between space and time dimensions. Such an *unstructured* discretization of the space-time domain [35] is the distinguishing feature of space-time discretization methods. The development of space-time finite element methods has already reached a certain degree of maturity, see e.g. [50, 69, 25, 51, 16, 72] and [18, 32, 33]. The major drawback of space-time methods is their increased demand in terms of computational resources compared to classical approaches based on semi-discretization. Nevertheless, space-time methods possess several crucial advantages:

- Flexible space-time meshes can adapt locally to special features of the solution, such as wave fronts. Adaptivity within space-time boundary element methods for the 1d wave equation is explored in [74, 54].
- Problems posed on instationary domains are treated naturally since the deformed configuration of the domain at any point in time is captured by the space-time mesh itself [50, 73].
- Treating the discretized transient problem as a single operator equation in space-time incites the development of parallel solution strategies, cf. [50, 25].

On the other hand, there has been hardly any development of space-time discretization schemes for time domain integral equations. The integral representations of these operators are quite involved, especially in the case of hyperbolic problems. However, there exist techniques for computing these integrals if space and time are treated separately [2, 28, 27]. The intricacy of computing integral operators for unstructured space-time decompositions is the reason why, almost any yet implemented discretization scheme for RPBEs features a product structure in space and time. To the best of our knowledge, the most successful attempt yet at abandoning this product structure are the “causal” shape functions introduced by Frangi [21]. In this approach, the lateral boundary of the space-time cylinder is decomposed into space-time slabs, which have a fixed substructure composed of simplices. The performed numerical experiments yield promising results. Although this approach does not enable completely unstructured space-time meshes, it can be seen as a precursor to them. Unstructured space-time meshes as well as

instationary boundaries in the context of integral equations of parabolic problems are examined in recent publications [46].

The novelty of this paper lies in the construction of genuine space-time approximations to RPBEs. The employed trial functions stem from standard finite element spaces defined on tetrahedral meshes of the lateral boundary of the space-time cylinder. This approach inherits the advantages of the space-time methodology, however, the integrals of the retarded layer potentials are quite complicated within this approach. That is why we restrict our considerations to collocation approaches, which we label space-time collocation schemes. The major part of this contribution is dedicated towards a numerical integration technique for the computation of the arising integrals. To the best of our knowledge, this paper provides the first implementation and numerical computations of a method for RPBEs in $3 + 1$ dimensions using unstructured space-time meshes.

The paper is organized as follows. In Section 2 the considered model initial-boundary value problem and related time domain boundary integral equations are discussed. Section 3 exposes the proposed space-time collocation method for the RPBEs of the preceding section. The standard integral representations of retarded layer integral operators are recast to a form appropriate for the chosen space-time trial functions. A numerical integration scheme for the occurring integrals is proposed. In Section 4 the integration technique and the overall collocation method are verified by means of numerical examples. Section 5 concludes this paper by summarizing the findings and addressing critical issues of the proposed approach.

2 Integral form of the wave equation

Let $\Omega^- \subset \mathbb{R}^3$ be a bounded open domain with Lipschitz boundary $\Gamma := \partial\Omega^-$ and exterior $\Omega^+ := \mathbb{R}^3 \setminus \overline{\Omega^-}$. The vector field $n : \Gamma \rightarrow \mathbb{R}^3$ represents the unit outward normal vector of Γ , which points towards Ω^+ . Moreover, let $c > 0$ be the wave velocity, e.g. the speed of sound. We employ the scaled time coordinate $t = ct^*$, where t^* is the physical time. Since t is the product of velocity and time its physical dimension is length. Nevertheless, we refer to the coordinate t as time from here on, since for every t there is exactly one corresponding physical time $t^* = c^{-1}t$. For a fixed physical simulation end time $T^* > 0$ we define $T = cT^*$ and the space-time cylinder $Q^+ := (0, T) \times \Omega^+$ with lateral boundary $\Sigma := (0, T) \times \Gamma$. We are concerned with solutions of the homogeneous wave equation

$$\partial_t^2 u - \Delta_x u = 0 \quad \text{in } Q^+ \quad (1)$$

where Δ_x denotes the the Laplacian with respect to the spatial coordinates. The solution is subject to homogeneous initial conditions

$$u = 0 \wedge \partial_t u = 0 \quad \text{on } \{0\} \times \Omega^+. \quad (2)$$

To impose boundary conditions we make use of the trace operator, which is for a sufficiently smooth function $f : Q^+ \rightarrow \mathbb{R}$ defined by

$$\gamma_0^+ f(t, x) = \lim_{y \in \Omega^+, y \rightarrow x} f(t, y), \quad (t, x) \in \Sigma.$$

Moreover, the normal derivative is denoted by

$$\gamma_1^+ f = \langle n, \gamma_0^+ \nabla_x f \rangle$$

where ∇_x is the gradient with respect to the spatial coordinates and $\langle \cdot, \cdot \rangle$ is the Euclidean scalar product with induced norm $\| \cdot \| = \sqrt{\langle \cdot, \cdot \rangle}$. We consider boundary conditions of Dirichlet type: For given Dirichlet datum g the solution u has to satisfy

$$\gamma_0^+ u = g \quad \text{on } \Sigma. \quad (3)$$

The solution of the initial-boundary value problem Eqs. (1) to (3) can be represented by boundary integrals in an elegant fashion, since they reduce the problem posed on the unbounded domain Q^+ to the bounded lateral boundary Σ . The main ingredient for a boundary integral formulation is the forward (causal) fundamental solution of the wave operator in Eq. (1) for three spatial dimensions [53, Ex. 1.4.12]

$$\mathcal{G}(t, x) = \frac{\delta_0(t - \|x\|)}{4\pi\|x\|} \quad (4)$$

where δ_0 denotes the Dirac delta function. For sufficiently smooth surface densities $w, v : \Sigma \rightarrow \mathbb{R}$ and $(t, x) \in Q^+$ the retarded single layer potential

$$\text{SL} w(t, x) = \int_{\Gamma} \int_0^T \mathcal{G}(t - \zeta, x - y) w(\zeta, y) d\zeta dS(y) = \int_{\Gamma} \frac{w(t - \|x - y\|, y)}{4\pi\|x - y\|} dS(y)$$

and the retarded double layer potential

$$\begin{aligned} \text{DL} v(t, x) &= \int_{\Gamma} \int_0^T \langle n(y), \nabla_y \mathcal{G}(t - \zeta, x - y) \rangle v(\zeta, y) d\zeta dS(y) \\ &= \int_{\Gamma} \frac{\langle n(y), x - y \rangle}{4\pi\|x - y\|^2} \left(\frac{v(t - \|x - y\|, y)}{\|x - y\|} + \partial_t v(t - \|x - y\|, y) \right) dS(y) \end{aligned}$$

satisfy Eqs. (1) and (2) if the densities are extended such that $w(t, \cdot) = 0$ and $v(t, \cdot) = 0$ for $t < 0$, see e.g. [12, 66]. Note that the name *retarded* is due to the property that these operators integrate their input densities along the retarded time $t - \|x - y\|$, which is elaborated in detail in Section 3. Applying the trace to the layer potentials induces the retarded single and double layer boundary integral operators

$$\gamma_0^+ \text{SL} = \mathbf{V} \quad , \quad \gamma_0^+ \text{DL} = \sigma \mathbf{I} + \mathbf{K}$$

where $\sigma : \Gamma \rightarrow \mathbb{R}$ is the solid angle or jump term [64, Eq. (3.3.11)]. For $(t, x) \in \Sigma$ the retarded single and double layer boundary integral operators have the representations

$$\mathbf{V} w(t, x) = \int_{\Gamma} \frac{w(t - \|x - y\|, y)}{4\pi\|x - y\|} dS(y) \quad (5)$$

and

$$\mathbf{K} v(t, x) = \int_{\Gamma} \frac{\langle n(y), x - y \rangle}{4\pi\|x - y\|^2} \left(\frac{v(t - \|x - y\|, y)}{\|x - y\|} + \partial_t v(t - \|x - y\|, y) \right) dS(y)$$

where the densities are extended by zero for $t < 0$. Solutions of Eqs. (1) and (2) are unambiguously defined by their Cauchy data $(\gamma_0^+ u, \gamma_1^+ u)$ via the representation formula, also known as Kirchhoff's formula

$$u = \text{DL } \gamma_0^+ u - \text{SL } \gamma_1^+ u. \quad (6)$$

In this work, we shall not use Eq. (6) to construct solutions of Eqs. (1) to (3) but we employ the ansatz $u := \text{SL } w$, satisfying Eqs. (1) and (2) for any suitable surface density w . To satisfy Eq. (3) the trace is applied to the ansatz yielding the boundary integral equation

$$\text{V } w = g \quad \text{on } \Sigma. \quad (7)$$

Once the solution of Eq. (7) is known $u = \text{SL } w$ yields the solution of Eqs. (1) to (3).

3 Space-time discretization of RPBIEs

To obtain approximate solutions of the boundary integral equation Eq. (7) we develop in this chapter a space-time collocation approach. To this end, the lateral boundary Σ is decomposed into a mesh Σ_N of $N \in \mathbb{N}$ open boundary elements τ with

$$\Sigma_N = \{\tau_\ell\}_{\ell=1}^N, \quad \tau_i \cap \tau_j = \emptyset \text{ for } i \neq j, \quad \bar{\Sigma} = \bigcup_{\tau \in \Sigma_N} \bar{\tau}.$$

The explicit choice of the geometric shape of the boundary elements is detailed in Section 3.2. The local and global mesh size are defined by

$$h_\tau := \text{diam } \tau, \quad h := \max_{\tau \in \Sigma_N} h_\tau.$$

Each boundary element is the image of the same reference element $\hat{\tau}$ under a smooth bijective parametrization $\chi_\tau : \hat{\tau} \rightarrow \tau$. The gradient of χ_τ induces the Jacobi matrix

$$\mathbb{R}^{4 \times 3} \ni J_\tau(\xi) := \nabla \chi_\tau(\xi) = (\partial_1 \chi_\tau(\xi) \quad \partial_2 \chi_\tau(\xi) \quad \partial_3 \chi_\tau(\xi))$$

whose columns are the three tangential vectors $\partial_i \chi_\tau(\xi), i = 1, 2, 3$. For non-degenerate boundary elements $\text{rank } J_\tau(\xi) = 3$ holds for all $\xi \in \hat{\tau}$. Consequently, the matrix

$$\mathbb{R}^{3 \times 3} \ni G_\tau(\xi) := J_\tau^\top(\xi) J_\tau(\xi) = (\langle \partial_i \chi_\tau(\xi), \partial_j \chi_\tau(\xi) \rangle)_{i,j=1}^3$$

is (symmetric) positive definite for all $\xi \in \hat{\tau}$. The kernel of J_τ^\top induces the space-time normal vector field $\mathbf{v} : \Sigma \rightarrow \mathbb{R}^4$ via

$$\ker J_\tau^\top(\xi) = \text{span}\{\mathbf{v} \circ \chi_\tau(\xi)\}.$$

For stationary domains, as introduced in Section 2 it holds for $(t, x) \in \Sigma$

$$\mathbf{v}(t, x) = \begin{pmatrix} v_t(t, x) \\ v_x(t, x) \end{pmatrix} = \begin{pmatrix} 0 \\ n(x) \end{pmatrix}$$

i.e. the time component v_t is zero and the spatial component v_x is just the normal vector of Γ .

To conclude this section, the employed trial spaces are discussed. In this work, standard finite element spaces, i.e. spaces of piecewise polynomial functions, on the mesh Σ_N are used. For simplicity we only consider the lowest-order trial spaces, namely the discontinuous trial space of piecewise constant functions

$$S_h^0(\Sigma_N) := \{v : \Sigma \rightarrow \mathbb{R} : v|_{\tau} \circ \chi_{\tau} \in \mathbb{P}^0(\hat{\tau}) \quad \forall \tau \in \Sigma_N\}$$

and the continuous trial space of hat functions

$$S_h^1(\Sigma_N) := \{v : \Sigma \rightarrow \mathbb{R} : v|_{\tau} \circ \chi_{\tau} \in \mathbb{P}^1(\hat{\tau}) \quad \forall \tau \in \Sigma_N\} \cap C(\Sigma).$$

These spaces are *space-time* trial spaces, since there is no inherent distinction between space and time coordinates. In order to collocate the boundary integral equation Eq. (7), evaluations of $V w_h(t, x)$ at $(t, x) \in \Sigma$ are necessary, where w_h is in one of the space-time trial spaces defined above. While integral representations of retarded potentials like Eq. (5) are suitable for classical methods that discretize space and time separately, they are inconvenient for capturing the action of retarded potentials on space-time trial functions. To this end, we derive a different representation of retarded potentials for the space-time mesh Σ_N in the following subsection.

3.1 Retarded potentials and space-time meshes

For convenience of notation we introduce an operator that unifies the integral representations of SL, DL, V, and K. For an arbitrary but fixed evaluation point $(t, x) \in [0, T] \times \mathbb{R}^3$ and surface density $w \in L^\infty(\Sigma)$ the abstract retarded potential integral operator T_k is defined by

$$\begin{aligned} T_k w(t, x) &= \int_{\Gamma} \int_0^T k(x, y) \delta_0(t - \zeta - \|x - y\|) w(\zeta, y) d\zeta dS(y) \\ &= \int_{\Gamma} k(x, y) w(t - \|x - y\|, y) dS(y) \end{aligned} \quad (8)$$

where $k : \mathbb{R}^3 \times \mathbb{R}^3 \rightarrow \mathbb{R}$ denotes the kernel function and w is extended trivially for negative times. For the three kernel functions of interest

$$k_1(x, y) = \frac{1}{4\pi\|x - y\|}, \quad k_2(x, y) = \frac{\langle n(y), x - y \rangle}{4\pi\|x - y\|^3}, \quad k_3(x, y) = \frac{\langle n(y), x - y \rangle}{4\pi\|x - y\|^2} \quad (9)$$

the integral Eq. (8) exists as weakly singular surface integral if $(t, x) \in \Sigma$, see [64, Th. 3.3.5, Lem. 3.3.8]. The operator T_k is identified with the operators of Section 2 via

$$V \leftrightarrow SL = T_{k_1}, \quad K \leftrightarrow DL = T_{k_2} + T_{k_3} \partial_t.$$

In order to recast Eq. (8) we introduce the function $\phi : \mathbb{R} \times \mathbb{R}^3 \rightarrow \mathbb{R}$

$$\phi(\zeta, y) = \|x - y\| - (t - \zeta)$$

whose zero level set

$$\Xi := \{(\zeta, y) \in \mathbb{R} \times \mathbb{R}^3 : \phi(\zeta, y) = 0\}$$

is a three-dimensional conical hypersurface embedded in four-dimensional space-time with apex at (t, x) and axis parallel to the time axis. This *backward light cone* is the support of the causal fundamental solution of the wave operator Eq. (4), see [52, Op. 51]. An illustration of the light cone in 2+1 dimensions is provided in Section 3.1.

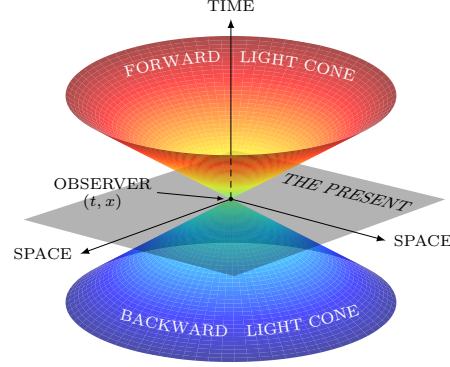


Figure 1: Visualization of the light cone in 2 + 1 dimensions. The observer at (t, x) perceives signals emitted on the backward light cone Ξ only. Conversely, a signal emitted at (t, x) is perceived only by observers on the forward light cone. This idea bestows a physical interpretation to retarded potentials, which integrate along the intersection of Ξ and the space-time boundary Σ , see Eq. (11b).

Using the (formal) representation of T_k with the delta function in Eq. (8) in conjunction with the decomposition Σ_N yields

$$\begin{aligned} T_k w(t, x) &= \int_{\Sigma} k(x, y) w(\zeta, y) \delta_0 \circ \phi(\zeta, y) dS(\zeta, y) \\ &= \sum_{\tau \in \Sigma_N} \int_{\hat{\tau}} k(x, \cdot) \circ |_x \chi_{\tau}(\xi) w \circ \chi_{\tau}(\xi) \delta_0 \circ \phi \circ \chi_{\tau}(\xi) \sqrt{\det G_{\tau}(\xi)} d\xi \end{aligned}$$

where $|_x \chi_{\tau}(\xi)$ denotes the restriction of the vector $\chi_{\tau}(\xi)$ to the spatial component only. By introducing the integrand

$$f_{\tau}(\xi) = k(x, \cdot) \circ |_x \chi_{\tau}(\xi) w \circ \chi_{\tau}(\xi) \sqrt{\det G_{\tau}(\xi)}$$

we obtain

$$T_k w(t, x) = \sum_{\tau \in \Sigma_N} \int_{\hat{\tau}} \delta_0 \circ \phi \circ \chi_{\tau}(\xi) f_{\tau}(\xi) d\xi. \quad (10)$$

To endow Eq. (10) with an intuitive interpretation, we shall use the coarea formula.

Theorem 3.1 (Coarea formula [19]). Let $\Omega \subset \mathbb{R}^d$, $d \geq 2$ be open, $g : \Omega \rightarrow \mathbb{R}$ be Lipschitz continuous and $f : \Omega \rightarrow \mathbb{R}$ be integrable. Then it holds

$$\int_{\Omega} f(x) \|\nabla g(x)\| dx = \int_{\mathbb{R}} \int_{x \in \Omega: g(x)=z} f(x) dS(x) dz.$$

Formally applying the coarea formula to Eq. (10) yields the desired integral representation

$$T_k w(t, x) = \sum_{\tau \in \Sigma_N} \int_{\mathbb{R}} \delta_0(z) \int_{\xi \in \hat{\tau}: \phi \circ \chi_\tau(\xi) = z} \frac{f_\tau(\xi)}{\|\nabla(\phi \circ \chi_\tau(\xi))\|} dS(\xi) dz \quad (11a)$$

$$= \sum_{\tau \in \Sigma_N} \int_{\chi_\tau^{-1}(\Xi \cap \tau)} k(x, \cdot) \circ|_x \chi_\tau(\xi) w \circ \chi_\tau(\xi) \frac{\sqrt{\det G_\tau(\xi)}}{\|\nabla(\phi \circ \chi_\tau(\xi))\|} dS(\xi). \quad (11b)$$

where $\chi_\tau^{-1}(\Xi \cap \tau) = \{\xi \in \hat{\tau} : \phi \circ \chi_\tau(\xi) = 0\}$ is the intersection of the backward light cone Ξ and the boundary element τ in terms of reference coordinates. Note that in order to apply Theorem 3.1 formally to Eq. (10) the function $\hat{\tau} \rightarrow \mathbb{R} : \xi \mapsto f_\tau(\xi) \|\nabla(\phi \circ \chi_\tau(\xi))\|^{-1}$ has to be integrable. While f_τ is integrable by assumption, the following lemma captures properties of $\xi \mapsto \nabla(\phi \circ \chi_\tau(\xi))$.

Lemma 3.1. For $\xi \in \hat{\tau}$ almost everywhere $\nabla(\phi \circ \chi_\tau(\xi)) = J_\tau^\top(\xi) \nabla \phi \circ \chi_\tau(\xi)$ and

$$\beta_2(\xi) \leq \|\nabla(\phi \circ \chi_\tau(\xi))\|^2 \leq 2\beta_4(\xi)$$

hold, where $0 = \beta_1(\xi) < \beta_2(\xi) \leq \beta_3(\xi) \leq \beta_4(\xi)$ are the eigenvalues of $J_\tau(\xi) J_\tau^\top(\xi)$.

The proof is only technical and carried out in Appendix A. By Lemma 3.1 we have $\xi \mapsto \|\nabla(\phi \circ \chi_\tau(\xi))\|^{-1} \in L^\infty(\hat{\tau})$. Consequently, the integrand in Eq. (11b) is integrable and the application of Theorem 3.1 to Eq. (10) is justified (in the claimed formal sense).

Representation Eq. (11b) strikingly shows that retarded layer potentials integrate over the intersection of the backward light cone Ξ and the lateral boundary Σ . Both Ξ and Σ are three-dimensional hypersurfaces embedded in \mathbb{R}^4 , hence, their (non-empty, non-degenerate) intersection is a two-dimensional surface. Clearly, the complexity of $\Xi \cap \tau$ is controlled by both the light cone Ξ and the boundary element τ . While the light cone is stringently dictated by the wave equation, the shape of the boundary elements is still to be specified. Since the goal of this paper is to take a first decisive step towards space-time discretizations of RPBIes, we restrict ourselves to boundary elements of simplest shape.

3.2 Piecewise flat boundary description

The simplest boundary elements are simplex elements, which are in this case tetrahedral surface elements. Any tetrahedron τ can be parametrized by the affine map $\chi : \hat{\tau} \rightarrow \tau$

$$\chi : \xi \mapsto \begin{pmatrix} t_0 \\ x_0 \end{pmatrix} + J\xi \quad (12)$$

with the constant Jacobi matrix $J \in \mathbb{R}^{4 \times 3}$ with $\text{rank } J = 3$. Here $(t_0, x_0^\top)^\top \in \mathbb{R} \times \mathbb{R}^3$ is the coordinate vector of the first vertex of the tetrahedron τ . Furthermore, the space-time normal vector \mathbf{v} with $\text{span}\{\mathbf{v}\} = \ker J^\top$ is also constant. The Jacobi matrix has the block structure $J^\top = (j_t \quad J_x^\top)$ where $j_t \in \mathbb{R}^3$ and $J_x \in \mathbb{R}^{3 \times 3}$ are the time and space components respectively. From $\mathbf{v}_t = 0$ it follows

$$0 = J^\top \mathbf{v} = j_t \mathbf{v}_t + J_x^\top \mathbf{n} = J_x^\top \mathbf{n}$$

which implies $1 = \dim \ker J_x^\top = \dim \ker J_x$ since J_x is a square matrix. Obviously, Eq. (12) is well-defined in the entire reference space \mathbb{R}^3 . This motivates to think of Eq. (12) as map $\chi : \mathbb{R}^3 \rightarrow \text{ran } \chi$ (ran denotes the range) and the parametrization of τ as the restriction $\chi|_{\hat{\tau}} : \hat{\tau} \rightarrow \tau$. From here on, χ shall always denote the extended affine map $\chi : \mathbb{R}^3 \rightarrow \text{ran } \chi$. Its range $\text{ran } \chi$ is a three-dimensional affine subspace of \mathbb{R}^4 . In other words, $\text{ran } \chi$ is the hyperplane induced by the normal vector ν of the flat element τ .

In order to construct an admissible tetrahedral mesh Σ_N we employ the algorithm outlined in [37]. In our case, the cited procedure uses a given admissible decomposition of Γ into triangles to build a tetrahedral mesh of Σ . Different strategies for generating space-time meshes can be found in [9, 20].

3.3 Intersection of light cone and flat boundary

Throughout the remainder of this section we consider an arbitrary but fixed point $(t, x) \in [0, T] \times \mathbb{R}^3$ and a tetrahedral boundary element $\tau \in \Sigma_N$ with affine parametrization $\chi : \mathbb{R}^3 \rightarrow \text{ran } \chi$. For simplicity of notation we omit the subscripts related to τ and introduce the metric signature $M := \text{diag}(-1, 1, 1, 1)$. The surface in Eq. (11b) can be rewritten as

$$\chi^{-1}(\Xi \cap \tau) = \{\xi \in \mathbb{R}^3 : \phi_2 \circ \chi(\xi) = 0\} \cap \{\xi \in \mathbb{R}^3 : |_t \chi(\xi) \leq t\} \cap \hat{\tau} \quad (13)$$

where $|_t \chi(\xi)$ denotes the restriction of the vector $\chi(\xi)$ to its time component and $\phi_2 : \mathbb{R} \times \mathbb{R}^3 \rightarrow \mathbb{R}$ is the quadratic level set function

$$\phi_2(\zeta, y) = \|x - y\|^2 - (t - \zeta)^2 = \left\langle M \begin{pmatrix} t - \zeta \\ x - y \end{pmatrix}, \begin{pmatrix} t - \zeta \\ x - y \end{pmatrix} \right\rangle.$$

In essence, Eq. (13) separates $\chi^{-1}(\Xi \cap \tau)$ into three components: The set $\{\xi : \phi_2 \circ \chi(\xi) = 0\}$ is the intersection of the hyperplane $\text{ran } \chi$ and the double light cone, i.e. both forward and backward portion, in terms of reference coordinates. The second part in Eq. (13) restricts to the backward light cone while the third part restricts to the actual boundary element. We shall study the zero level set of $\phi_2 \circ \chi$ and recall that $\chi^{-1}(\Xi \cap \tau)$ is a certain subset of it.

Insertion of the affine parametrization Eq. (12) yields the quadratic equation

$$\phi_2 \circ \chi(\xi) = \langle A \xi, \xi \rangle + 2 \langle b, \xi \rangle + c_0$$

with $A \in \mathbb{R}^{3 \times 3}$, $b \in \mathbb{R}^3$, $c_0 \in \mathbb{R}$, and $z_0 \in \mathbb{R}^4$ defined by

$$A := J^\top M J, \quad b := -J^\top M z_0, \quad c_0 := \langle M z_0, z_0 \rangle, \quad z_0 := \begin{pmatrix} t - t_0 \\ x - x_0 \end{pmatrix}.$$

Since A is symmetric its eigenvalues are real and its eigenvectors form an orthonormal basis. Let the i th column of $E \in \mathbb{R}^{3 \times 3}$ be the i th eigenvector of A associated to the eigenvalues $\lambda_1 \leq \lambda_2 \leq \lambda_3$. With the matrix $D := \text{diag}(\lambda_i)_{i=1}^3$ the diagonalization $A = E D E^\top$ is obtained. We introduce the affine map $\kappa : \mathbb{R}^3 \rightarrow \mathbb{R}^3$

$$\kappa(\eta) = \xi_0 + E \eta$$

with the origin $\xi_O = -A^{-1}b$ and get the quadratic equation in principal axes

$$\phi_2 \circ \chi \circ \kappa(\eta) = \sum_{i=1}^3 \lambda_i \eta_i^2 + c_M \quad (14)$$

where $c_M := \langle b, \xi_O \rangle + c_0$. Obviously ξ_O is well-defined iff A is invertible. The following lemma enables a categorization of Eq. (14).

Lemma 3.2. It holds $\lambda_1 < 0 < \lambda_2 \leq \lambda_3$ and $c_M = \langle z_0, v \rangle^2 = \langle x - x_0, n \rangle^2$.

The proof of this lemma is merely technical and deferred to Appendix A. From Lemma 3.2 we observe that $c_M = 0$ iff $\langle z_0, v \rangle = 0$. This is the case iff $(t, x) \in \text{ran } \chi$, i.e. the apex of the light cone at (t, x) lies in the hyperplane $\text{ran } \chi$. From Lemma 3.2 it follows that the zero set of Eq. (14) and hence $\{\xi : \phi_2 \circ \chi(\xi) = 0\}$ is an elliptic hyperboloid of two sheets if $(t, x) \notin \text{ran } \chi$ or an elliptic double cone if $(t, x) \in \text{ran } \chi$. One sheet of the hyperboloid or one cone of the double cone is associated to the forward light cone and consequently not of interest for Eq. (13). To ensure that $\eta_1 > 0$ is associated to the backward light cone, the eigenvector e_1 with eigenvalue $\lambda_1 < 0$ is oriented such that

$$\langle e_1, j_t \rangle < 0 \quad (15)$$

where we recall that j_t is the first column of J^\top .

As next step Eq. (11b) is transformed to an integral in a parameter domain of the light cone in reference coordinates. The employed parametrization is available for flat boundary elements as discussed previously. The integral in Eq. (11b) is abbreviated

$$\mathcal{I} := \int_{\chi^{-1}(\Xi \cap \tau)} k_x(\xi) w_{\hat{\tau}}(\xi) dS(\xi) \quad (16)$$

where

$$k_x(\xi) = k(x, \cdot) \circ|_x \chi(\xi), \quad w_{\hat{\tau}}(\xi) = w \circ \chi(\xi) \frac{\sqrt{\det G}}{\|\nabla(\phi \circ \chi(\xi))\|}, \quad \xi \in \hat{\tau}.$$

The key ingredients of the employed transformation are well-known parametrizations of the cone/hyperboloid. The backward cone is parametrized by

$$\begin{aligned} \psi_C : [0, 2\pi) \times [0, \infty) &\rightarrow \mathbb{R}^3 \\ \begin{pmatrix} \rho_1 \\ \rho_2 \end{pmatrix} &\mapsto \sqrt{-\lambda_1} \rho_2 \begin{pmatrix} \frac{1}{\sqrt{-\lambda_1}} \\ \frac{1}{\sqrt{\lambda_2}} \cos \rho_1 \\ \frac{1}{\sqrt{\lambda_3}} \sin \rho_1 \end{pmatrix} \end{aligned}$$

while the backward sheet of the two-sheeted hyperboloid is parametrized by

$$\begin{aligned} \psi_H : [0, 2\pi) \times [0, \infty) &\rightarrow \mathbb{R}^3 \\ \begin{pmatrix} \rho_1 \\ \rho_2 \end{pmatrix} &\mapsto \sqrt{c_M} \cosh \rho_2 \begin{pmatrix} \frac{1}{\sqrt{-\lambda_1}} \\ \frac{1}{\sqrt{\lambda_2}} \tanh \rho_2 \cos \rho_1 \\ \frac{1}{\sqrt{\lambda_3}} \tanh \rho_2 \sin \rho_1 \end{pmatrix} \end{aligned}$$

and the desired parametrization is defined by

$$\psi := \begin{cases} \kappa \circ \psi_C & c_M = 0 \\ \kappa \circ \psi_H & c_M > 0 \end{cases}$$

where Eq. (15) ensures that ψ maps onto the backward portion of the light cone only. We introduce $\text{dom } \psi := [0, 2\pi) \times [0, \infty)$ (dom denotes the domain) and by construction $\text{ran } \psi = \chi^{-1}(\Xi \cap \text{ran } \chi)$ holds. This allows us to carry the integral Eq. (16) over to an integral in $\text{dom } \psi$

$$\mathcal{I} = \int_{\Theta} k_x \circ \psi(\rho) w_{\hat{\tau}} \circ \psi(\rho) g_{\psi}(\rho) d\rho \quad (17)$$

with $\Theta := \{\rho \in \text{dom } \psi : \psi(\rho) \in \hat{\tau}\} = \psi^{-1}(\hat{\tau} \cap \text{ran } \psi)$ and

$$g_{\psi}(\rho) = \left(\det \left(\langle \partial_i \psi(\rho), \partial_j \psi(\rho) \rangle \right)_{i,j=1}^2 \right)^{1/2}.$$

In this context, we use the notation ψ^{-1} in a formal sense, since ψ is not injective on $\text{dom } \psi$ but only on the dense subset $[0, 2\pi) \times (0, \infty)$. The parametrization of the light cone in reference coordinates is depicted in Section 3.3. Our goal is to employ numerical integration based on Gaussian quadrature rules to approximate Eq. (17). Representation Eq. (17) is advantageous for this purpose because the product of kernel function and transformation determinant defines a smooth function.

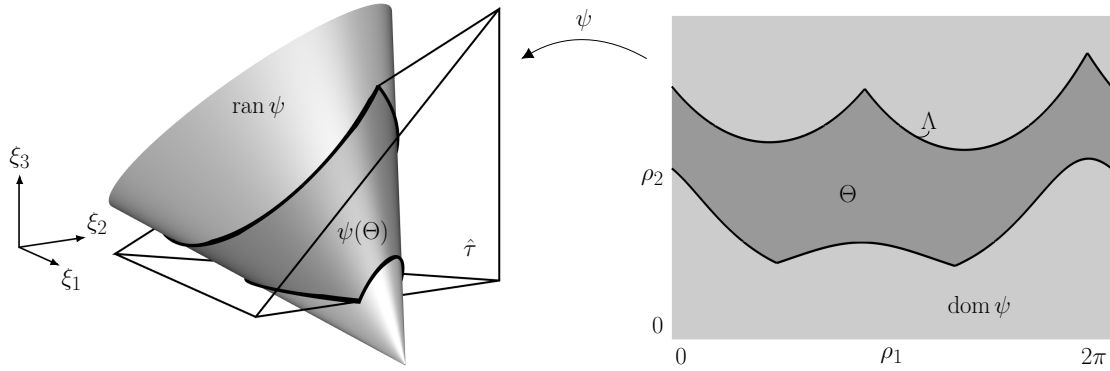


Figure 2: Sketch of the parametrization of the light cone in reference coordinates of a tetrahedral boundary element.

Lemma 3.3. For any $\rho \in \text{dom } \psi$ it holds

$$g_{\psi}(\rho) = \begin{cases} -\lambda_1 \rho_2 g_C(\rho) & c_M = 0 \\ c_M \sinh \rho_2 \cosh \rho_2 g_H(\rho) & c_M > 0 \end{cases}$$

where $g_C, g_H : \text{dom } \psi \rightarrow \mathbb{R}$ are smooth and $0 < (\lambda_2 \lambda_3)^{-1/2} \leq g_H(\rho) < g_C(\rho)$. Moreover, let $d_x(y) = \|x - y\|$ for any $x, y \in \mathbb{R}^3$. For any $\rho \in \text{dom } \psi$

$$d_x \circ |_{\chi} \chi \circ \psi(\rho) = \begin{cases} \sqrt{-\lambda_1} \rho_2 f_C(\rho) & c_M = 0 \\ \sqrt{c_M} \cosh \rho_2 f_H(\rho) & c_M > 0 \end{cases}$$

where $f_C, f_H : \text{dom } \psi \rightarrow \mathbb{R}$ are smooth and bounded from below by a positive constant.

The proof is given in Appendix A.

Theorem 3.2. Let $k_i, i = 1, 2, 3$ be the functions as in Eq. (9). For any $x \in \mathbb{R}^3$ the function $k_i^*(\rho) = k_i(x, \cdot) \circ|_x \chi \circ \psi(\rho) g_\psi(\rho)$ can be extended to $C^\infty(\mathbb{R} \times [0, \infty))$.

Proof. As discussed in Section 3.2 it holds $J_x^\top n = 0$. From Lemma 3.2 we have $c_M = \langle n, x - x_0 \rangle^2$ and for any $\xi \in \mathbb{R}^3$

$$\langle n, x -|_x \chi(\xi) \rangle^2 = \langle n, x - x_0 - J_x \xi \rangle^2 = \langle n, x - x_0 \rangle^2 = c_M$$

follows. For any $\rho \in \mathbb{R} \times [0, \infty)$ the map ψ is well-defined and takes values in $\text{ran } \psi$ due to periodicity in the first component. Consider the functions $k_i^* : \mathbb{R} \times [0, \infty) \rightarrow \mathbb{R}$ defined by $k_i^* : \rho \mapsto k_i(x, \cdot) \circ|_x \chi \circ \psi(\rho) g_\psi(\rho)$, where $k_i, i = 1, 2, 3$ is as in Eq. (9) apart from the division by 4π . There hold the representations for $c_M = 0$

$$k_1^*(\rho) = \sqrt{-\lambda_1} \frac{g_C(\rho)}{f_C(\rho)}, k_2^*(\rho) = 0, k_3^*(\rho) = 0$$

and for $c_M > 0$ with $s_x := \text{sgn} \langle n, x - x_0 \rangle \neq 0$

$$k_1^*(\rho) = \sqrt{c_M} \sinh \rho_2 \frac{g_H(\rho)}{f_H(\rho)}, k_2^*(\rho) = s_x \frac{\tanh \rho_2}{\cosh \rho_2} \frac{g_H(\rho)}{f_H^3(\rho)}, k_3^*(\rho) = s_x \sqrt{c_M} \tanh \rho_2 \frac{g_H(\rho)}{f_H^2(\rho)}$$

with f_X, g_X for $X \in \{C, H\}$ as in Lemma 3.3. The smoothness of above functions is an immediate consequence of Lemma 3.3 which concludes the proof. \square

Theorem 3.2 conveys that the transformation induced by ψ regularizes the potentially weakly singular integral Eq. (16), which is a decisive advantage of representation Eq. (17). To enable the application of existing numerical integration techniques, we recast Θ to an implicitly defined set. The reference tetrahedron $\hat{\tau}$ is the intersection of four open half spaces. Let $d_i : \mathbb{R}^3 \rightarrow \mathbb{R}$ for $i = 1, \dots, 4$ be the signed distance function of the plane that defines the i th half space. With the continuous function

$$\phi_{\hat{\tau}} : \mathbb{R}^3 \rightarrow \mathbb{R}, \xi \mapsto \max_{i=1, \dots, 4} \{d_i(\xi)\}$$

we can provide the equivalent definition

$$\Theta = \{\rho \in \text{dom } \psi : \phi_{\hat{\tau}} \circ \psi(\rho) < 0\}. \quad (18)$$

There exist several methods for approximating the integral Eq. (17) with the implicitly defined set Eq. (18). Prominent approaches are based on (high-order) approximations of the implicitly defined set [38, 23, 24], moment-fitting techniques [49], and local parametrizations [67]. Although these procedures can yield reliable results for Eq. (17), we shall provide an approach tailored to the situation at hand.

Remark 1. Although this work deals with stationary boundaries, several results can indeed be generalized to instationary ones. Under the assumption that the normal velocity of the boundary element is lower than the speed of wave propagation, similar versions of Lemmas 3.1 and 3.2 hold true, implying that the hyperconic section $\Xi \cap \text{ran } \chi$ remains a cone/hyperboloid. We do not provide these results here, as the focus of this paper lies on the space-time methodology itself rather than instationary domains.

3.4 A quadrature scheme for \mathcal{I}

In the following paragraphs a numerical integration technique for evaluating Eq. (17) is devised. The integral \mathcal{I} is recast into a sum of integrals over a simple reference interval, which are treated by standard Gaussian quadrature. For ease of notation we abbreviate the integrand

$$k_\psi(\rho) = k_x \circ \psi(\rho) w_{\hat{\tau}} \circ \psi(\rho) g_\psi(\rho), \quad \rho \in \Theta$$

and introduce the integrated kernel

$$k_\psi^+(\rho_1, \rho_2) = \int_0^{\rho_2} k_\psi(\rho_1, r) dr = \rho_2 \int_0^1 k_\psi(\rho_1, \rho_2 r) dr, \quad (\rho_1, \rho_2) \in \overline{\Theta}. \quad (19)$$

Note that Eq. (19) is well-defined only if there exists a suitable extension of k_ψ outside of Θ . By Theorem 3.2, the product of $k_x \circ \psi$ and g_ψ defines a smooth function in $\text{dom } \psi$. A straightforward computation confirms that $\nabla(\phi \circ \chi_\tau) \circ \psi$ is smooth and in conjunction with Lemma 3.1 it follows that $\rho \mapsto \|\nabla(\phi \circ \chi_\tau) \circ \psi(\rho)\|^{-1}$ is a smooth function in $\text{dom } \psi$ as well. In practical computations $w|_\tau \circ \chi$ is a polynomial basis function, for which the extension to an entire function is obvious. Hence, we may assume that Eq. (19) is well-defined and its integrand is smooth. As a consequence, we may apply the divergence theorem, which yields

$$\mathcal{I} = \int_{\partial\Theta} k_\psi^+(\rho) n_2^\Theta(\rho) dS(\rho) = \int_\Lambda k_\psi^+(\rho) n_2^\Theta(\rho) dS(\rho) \quad (20)$$

where n_2^Θ denotes the ρ_2 -component of the unit outward normal vector field to Θ and

$$\Lambda := \{\rho \in \text{dom } \psi : \phi_{\hat{\tau}} \circ \psi(\rho) = 0\} = \psi^{-1}(\partial\hat{\tau} \cap \text{ran } \psi) \subseteq \partial\Theta.$$

Although Λ can be a subset of $\partial\Theta$, the second equality in Eq. (20) holds since integrals on $\{0, 2\pi\} \times [0, \infty)$ and $[0, 2\pi) \times \{0\}$ vanish, as either n_2^Θ or k_ψ^+ vanishes. In a certain sense, Eq. (20) reduces \mathcal{I} to an integral along the curve Λ , as only a parametrization of Λ is necessary to enable the application of standard quadrature schemes. We employ piecewise smooth parametrizations as discussed in [39], a closely related approach is proposed in [26]. The technique is reiterated here for the sake of completeness. Assume that we are given a piecewise affine interpolation Λ_1 of Λ . Each line $\sigma \in \Lambda_1$ is defined by its two end points $\rho_\sigma^A, \rho_\sigma^B \in \Lambda$ and parametrized by the affine map $\ell_\sigma : (0, 1) \rightarrow \sigma$. For some fixed width $\varepsilon > 0$ let $\Theta_\varepsilon := \{\rho \in \text{dom } \psi : \text{dist}(\rho, \Lambda) \leq \varepsilon\}$ be a strip around Λ . As in [39] we consider the transformation $\iota : \Theta_\varepsilon \rightarrow \Lambda$ defined by

$$\iota(\rho) = \rho + d(\rho)s(\rho) \quad (21)$$

with search direction field $s : \Theta_\varepsilon \rightarrow \mathbb{R}^2$ and the the function $d : \Theta_\varepsilon \rightarrow \mathbb{R}$. We use $s(\rho) = \nabla(\phi_{\hat{\tau}} \circ \psi(\rho))$ and $d(\rho)$ is the solution with smallest absolute value of

$$d(\rho) \in \mathbb{R} : \phi_{\hat{\tau}} \circ \psi(\rho + d(\rho)s(\rho)) = 0, \quad \rho \in \Theta_\varepsilon. \quad (22)$$

This transformation mimics the closest point projection, cf. [17, 26]. A parametrization of a subset of Λ is obtained by $\iota_\sigma := \iota \circ \ell_\sigma$ for $\sigma \in \Lambda_1$. Note that Eq. (21) is well-defined only if

ε is sufficiently small. To ensure that the line σ lies in Θ_ε it has to be sufficiently close to Λ , which implies that Λ_1 has to be sufficiently close to Λ . The construction of Λ_1 is discussed in Appendix B. Here, we assume that

$$\bar{\Lambda} = \bigcup_{\sigma \in \Lambda_1} \overline{\text{ran } \iota_\sigma} \quad \wedge \quad \text{ran } \iota_\sigma \cap \text{ran } \iota_\mu = \emptyset, \sigma \neq \mu \in \Lambda_1$$

and that ι_σ is injective for all $\sigma \in \Lambda_1$. This gives rise to the transformed integral

$$\mathcal{J} = \sum_{\sigma \in \Lambda_1} \int_0^1 k_\psi^+ \circ \iota_\sigma(r) n_2^\ominus \circ \iota_\sigma(r) \|\iota_\sigma'(r)\| dr. \quad (23)$$

By Eqs. (19) and (23) the evaluation of Eq. (17) is performed only by computation of integrals in the interval $(0, 1)$. The integrands are smooth if ι_σ is smooth and we suggest to approximate the integral by Gaussian quadrature rules. Notice that the integrand in Eq. (19) is (in general) not analytic everywhere. Although this lack of analyticity prevents Gaussian quadrature schemes from reaching their optimal convergence properties, they still yield acceptable approximations.

In our implementation of the algorithm, the integrals Eqs. (19) and (23) are approximated by Gauss-Legendre quadrature rules with $n_G \in \mathbb{N}$ integration points. The interval of integration in Eq. (19) is set to (α, ρ_2) with a suitable $\alpha \geq 0$, instead of $(0, \rho_2)$. Moreover, the non-linear equation Eq. (22) is solved by Newton's method [39, 26, 55] with initial guess $d(\rho) = 0$. In the examples reported in Section 4 at most 10 iterations in Newton's method were necessary to satisfy Eq. (22) up to machine precision.

3.5 Collocation method

To set up collocation equations of Eq. (7), we choose collocation points which are typically used in boundary element methods for elliptic problems. For $w_h \in S_h^0(\Sigma_N)$ the set of centroids of all elements $\mathcal{C}(\Sigma_N)$ is employed as set of collocation nodes, leading to the discretized boundary integral equation

$$w_h \in S_h^0(\Sigma_N) : \mathbf{V} w_h(t, x) = g(t, x), \quad (t, x) \in \mathcal{C}(\Sigma_N). \quad (24)$$

A problem somewhat similar to Eq. (24) is analyzed by Davies and Duncan [13]. In the cited paper, it is assumed that Γ is flat and the employed trial functions are products of functions in the spatial coordinates and functions in the time variable. The authors prove convergence of the solution of the arising collocation equations for certain trial spaces. However, they indicate that piecewise constant spatial basis functions yield unstable methods for a variety of mesh ratios. Since the trial functions in our approach are either continuous or discontinuous in space-time, we shall also consider approximations in $S_h^1(\Sigma_N)$. For $w_h \in S_h^1(\Sigma_N)$ the set of vertices of the mesh $\mathcal{V}(\Sigma_N)$ is chosen as set of collocation points. For continuous solutions of Eqs. (1) to (3) the Dirichlet data g has to be compatible with the initial data, in particular $g = 0$ on $\{0\} \times \Gamma$ has to hold. If the continuous density w_h can be continuously extended by zero for negative times it follows $w_h = 0$ on $\{0\} \times \Gamma$. This gives rise to the subspace

$$S_{h,0}^1(\Sigma_N) := \{v \in S_h^1(\Sigma_N) : v = 0 \text{ on } \{0\} \times \Gamma\}$$

and the subset of vertices which serve as collocation points

$$\mathcal{V}_0(\Sigma_N) := \{(t, x) \in \mathcal{V}(\Sigma_N) : t > 0\}.$$

This yields a discretization of Eq. (7) based on continuous basis functions

$$w_h \in S_{h,0}^1(\Sigma_N) : \mathbb{V} w_h(t, x) = g(t, x), \quad (t, x) \in \mathcal{V}_0(\Sigma_N). \quad (25)$$

To implement these boundary element discretizations, point-wise evaluations of retarded layer operators acting on space-time trial functions are required. On the one hand, evaluations of $\mathbb{V} w_h(t, x)$ for $(t, x) \in \Sigma$ are necessary to set up the left hand sides in Eqs. (24) and (25). On the other hand, approximate solutions of Eqs. (1) to (3) are obtained by evaluating $\text{SL} w_h(t, x)$ for $(t, x) \in Q^+$. Both of these evaluations are realized by means of the numerical integration scheme introduced in Section 3.4.

Remark 2. The outlined collocation methods can be interpreted as a preparatory step for space-time Galerkin discretizations. In this remark we provide an idea about the utilization of the proposed scheme in the context of space-time Galerkin schemes. A variational formulation of Eq. (7) is to find

$$w \in X : b(w, v) = \ell(v) \quad \forall v \in X$$

where X is a Hilbert space, see [12, Th. 3], [66, Ch. 3.7]. The bilinear form reads

$$b(w, v) = \int_{\Sigma} \omega(t) \mathbb{V} w(t, x) \partial_t v(t, x) dS(t, x)$$

and the functional

$$\ell(v) = \int_{\Sigma} \omega(t) g(t, x) \partial_t v(t, x) dS(t, x)$$

where $\omega \in C^1(0, T)$ is a suitable weight function [36]. Let $X_h \subset X$ be a space-time boundary element space, e.g. $S_h^0(\Sigma_N)$, with basis $\{\varphi_i\}_i$. If g and ω are smooth the numerical evaluation of $\ell(\varphi_i)$ is straightforward. However, the matrix entry

$$V_{ij} = \sum_{\tau \in \Sigma_N : \tau \subset \text{supp}(\varphi_i)} \int_{\tau} \omega(t) \mathbb{V} \varphi_j(t, x) \partial_t \varphi_i(t, x) dS(t, x)$$

is quite challenging to compute. We suggest to employ a suitable numerical integration technique which computes an approximation of the form

$$\int_{\tau} \omega(t) \mathbb{V} \varphi_j(t, x) \partial_t \varphi_i(t, x) dS(t, x) \approx \sum_{\ell=1}^{n_G} \omega(t_{\ell}) \mathbb{V} \varphi_j(t_{\ell}, x_{\ell}) \partial_t \varphi_i(t_{\ell}, x_{\ell}) \mathfrak{g}_{\ell} \quad (26)$$

where (t_{ℓ}, x_{ℓ}) and \mathfrak{g}_{ℓ} for $\ell = 1, \dots, n_G$ are quadrature points and weights respectively. In this context, the point-wise evaluation of the retarded potential integral operator

$$\tau \rightarrow \mathbb{R} : (t, x) \mapsto \mathbb{V} \varphi_j(t, x)$$

at the quadrature points can be performed accurately by the technique developed in Sections 3.3 and 3.4 without any modifications. Nevertheless, an accurate quadrature rule for Eq. (26) is required. In [70, Th. 1] a somewhat similar integral is analyzed, which arises in classical Galerkin discretizations based on product-type trial spaces. It is shown that the integrand features certain singularities. A similar behaviour is to be expected by the integrand in Eq. (26). The construction of an accurate quadrature scheme for Eq. (26) is, at least from our point of view, the pivotal step towards a practical realization of genuine space-time Galerkin discretization methods for RPBEs.

4 Numerical experiments

In this section the proposed method is verified by investigating elementary examples. In particular, the performance of the numerical integration technique as well as the overall space-time scheme is examined. To this end, we construct a simple, yet smooth solution of the wave equation. Consider a fixed source point $y_S \in \Omega^-$ and a sufficiently smooth signal $\mu : \mathbb{R} \rightarrow \mathbb{R}$ with $\text{supp } \mu \subset [0, \infty)$. The spherical wave function $f : \mathbb{R} \times (\mathbb{R}^3 \setminus y_S) \rightarrow \mathbb{R}$

$$f(t, x) = \frac{\mu(t - \|x - y_S\|)}{\|x - y_S\|}$$

satisfies the wave equation subject to homogeneous initial conditions everywhere in its domain. Consequently, the restriction $u := f|_{Q^+}$ solves Eqs. (1) and (2). We consider

$$\mu(s) = \begin{cases} \exp\left(\left(\frac{s^2}{4} - s\right)^{-1}\right) & s \in (0, 4) \\ 0 & \text{otherwise} \end{cases}$$

which satisfies $\mu \in C^\infty(\mathbb{R})$. In all tests we use the source point $y_S = -(\frac{1}{10}, \frac{2}{10}, \frac{3}{10})^\top$, which is suitable for all examined scenarios.

4.1 Verification of the quadrature technique

The first test is intended to verify the numerical integration procedure for retarded potentials. As computational domain we consider the unit cube $\Omega^- = (-\frac{1}{2}, \frac{1}{2})^3$ with $T = 5$. Our goal is to evaluate

$$\tilde{u}(t, x) := \begin{cases} \widetilde{\text{DL}}\gamma_0^+ u(t, x) - \widetilde{\text{SL}}\gamma_1^+ u(t, x) & (t, x) \in Q^+ \\ \sigma(x)\gamma_0^+ u(t, x) + \widetilde{\text{K}}\gamma_0^+ u(t, x) - \widetilde{\text{V}}\gamma_1^+ u(t, x) & (t, x) \in \Sigma \end{cases} \quad (27)$$

which is Kirchhoff's formula Eq. (6) for $(t, x) \in Q^+$ or its trace for $(t, x) \in \Sigma$. The tildes over the integral operators should indicate that they are approximated by numerical integration. Since a mesh is necessary to run the integration algorithm we employ a uniform decomposition of Σ into 180 tetrahedrons ($h \approx 1.732$). However, the exact Cauchy data $(\gamma_0^+ u, \gamma_1^+ u)$ are used in Eq. (27) rather than mere approximations of them. The fact that we input the exact Cauchy data into the representation formula implies that the use of a mesh does not constitute an approximation.

The only approximation is due to the numerical integration in the retarded potentials by an order $n_G \in \mathbb{N}$ quadrature scheme as devised in Section 3.4. The error is measured by computing

$$e_n = \frac{|u(T, x) - \tilde{u}(T, x)|}{|u(T, x)|}$$

at the sampling point

$$x := \left(\frac{1}{2}, \frac{1}{2}, \frac{1}{2}\right)^\top + r(1, 0, 0)^\top$$

where $0 \leq r = \text{dist}(x, \Gamma)$. The results for different values of r are depicted in Fig. 3a. It can be observed that the quadrature error decays rapidly as the number of integration points is increased. Convergence ceases at $e_n \approx 10^{-14}$ since this value is already quite close to the employed machine precision. Furthermore, there is little dependence on the distance of the evaluation point to the boundary. In particular, the case $r = 0$, in which integral operators with weakly singular kernels are evaluated, is handled as well as the cases with positive distance. This is due to the parametrization introduced in Section 3.3, which regularizes the integrand, see Theorem 3.2. We note that the stated observations are quite comparable to numerical results provided in the literature. In [61, Fig. 3] and [63, Fig. 3.3] an integral with smooth (but not analytic) kernel, which arises in a Galerkin discretization of RPBIEs, is approximated by Gaussian quadrature. The quadrature errors observed in the cited references feature a similar behaviour to our experiment.

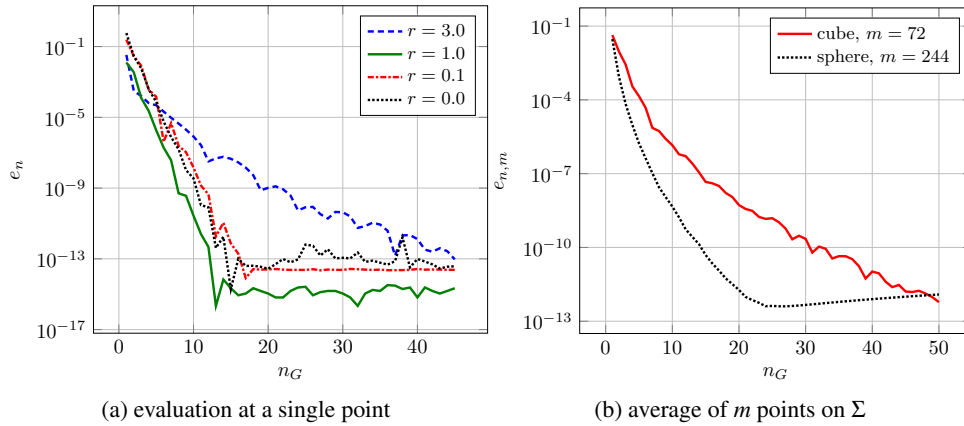


Figure 3: Convergence study of Eq. (27) for increasing quadrature order. Left: Evaluation of Kirchhoff's formula ($r > 0$) or the weakly singular boundary integral equation ($r = 0$) at a single point. Right: Weakly singular boundary integral equation, average of m evaluation points located on Σ .

In the previous example the space-time mesh is fixed and the convergence with respect to the number of quadrature points is examined. In the second test we study the reverse scenario: The number of quadrature points is fixed and the mesh is refined successively. Figure 4a exhibits the observed errors for $r = 1$ and Fig. 4b for $r = 0$. Note that in the algorithm devised in this work the total number of quadrature points does not scale rigidly with mesh refinement. Nevertheless, roughly second-order convergence with respect to h is observed. This indicates

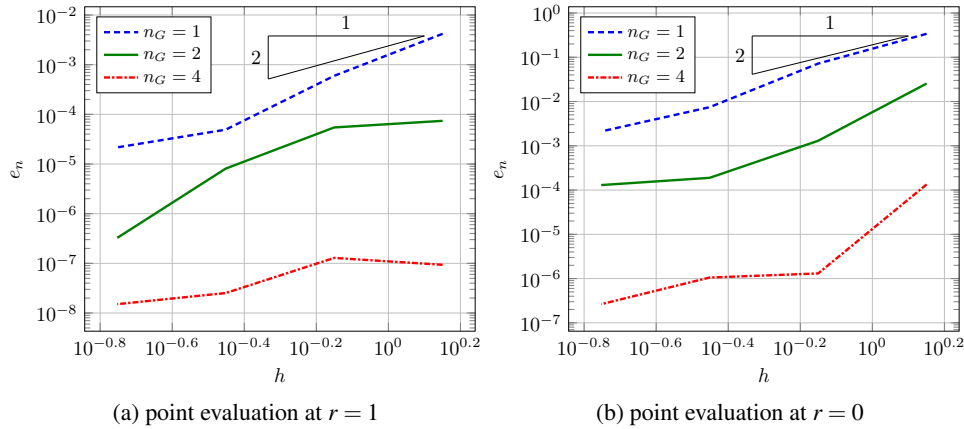


Figure 4: Convergence study of Eq. (27) for a sequence of successively refined uniform meshes.

that for sufficiently large n_G the error is dominated by mesh refinement, see [26, Fig. 5] for similar results.

We consider a further example to support the viability of the developed quadrature scheme for weakly singular kernel functions. Again Eq. (27) is evaluated, however, evaluation points exclusively on the boundary are of interest in this test. We fix a set of points $\{(t_i, x_i)\}_{i=1}^m$ with $(t_i, x_i) \in \Sigma, i = 1, \dots, m$ for $m \in \mathbb{N}$. The error measure

$$e_{n,m} = \frac{\sum_{i=1}^m |u(t_i, x_i) - \tilde{u}(t_i, x_i)|}{\sum_{i=1}^m |u(t_i, x_i)|}$$

is computed. We set $T = 5$ and study the two scenarios:

- *Cube*: Let $\Omega^- = (-\frac{1}{2}, \frac{1}{2})^3$ be decomposed into a mesh of 288 elements ($h \approx 1.546$). The error is evaluated at the $m = 72$ vertices of the mesh.
- *Sphere*: We consider $\Omega^- = \{x \in \mathbb{R}^3 : \|x\| < 1\}$, however, the employed mesh consisting of 5490 elements ($h \approx 0.674$) does not represent an exact sphere, but a polyhedral approximation of it. The error is computed at the $m = 244$ centroids of the elements with time coordinate $t > T - h/3$. This condition is used to ensure that the number of evaluation points is similar to the cube.

From the results exhibited in Fig. 3b one can infer that the error decays swiftly, especially in the pre-asymptotic regime. As expected by the lack of analyticity of the integrand, the error does however not decay at an exponential rate, cf. [63]. For the spherical domain we observe divergence at $e_{n,m} \approx 10^{-12}$ since roundoff errors are dominating the overall error. The sphere is composed of significantly more boundary elements than the cube. Therefore, the sphere uses many more integration points than the cube (for the same value of n_G) to compute the integral operators along its space-time boundary. That is why the error for the spherical domain is considerably smaller. Still, it decays substantially faster than conjectured.

These observations support the conclusion that the proposed numerical integration technique is indeed capable of computing accurate point-wise evaluations of retarded potential integral operators in the context of space-time meshes.

4.2 Verification of collocation schemes

In the following experiments the space-time collocation methods Eqs. (24) and (25) are tested.

4.2.1 Accuracy of linear systems

The discussed methods lead to a linear system of equations with matrix $V \in \mathbb{R}^{m \times m}$ where $m \in \mathbb{N}$ is the number of degrees of freedom. Prior to testing the actual methods it seems reasonable to investigate what quadrature orders are necessary to achieve accurate approximations of V . To this end, we compute collocation matrices V_n where $n \in \mathbb{N}$ is the order of quadrature used to approximate the retarded potential integral operator. We consider the unit cube $\Omega^- = (-\frac{1}{2}, \frac{1}{2})^3$ with $T = 5$. The matrices of both methods Eqs. (24) and (25) are set up for two meshes, composed of 504 ($h \approx 1.229$) and 4032 ($h \approx 0.615$) elements respectively. As reference, we employ extraordinarily many quadrature points to set up the matrix $V_{\bar{n}}$. The two error measures

$$e_n^F = \frac{\|V_{\bar{n}} - V_n\|_F}{\|V_{\bar{n}}\|_F}, \quad e_n^S = \frac{\|V_{\bar{n}} - V_n\|_2}{\|V_{\bar{n}}\|_2}$$

are computed, where $\|\cdot\|_F$ denotes the Frobenius norm and $\|\cdot\|_2$ the spectral norm. All tests are performed for $\bar{n} = 31$ and $\bar{n} = 61$, however, the results are indistinguishable. Consequently, only the results for $\bar{n} = 61$ are exhibited in Fig. 5a for method Eq. (24) and Fig. 5b for approach Eq. (25). The error decays rapidly in both norms and for both methods. Moreover, the error is virtually the same for both examined meshes. These findings suggest that the quadrature scheme is capable of computing accurate approximations of the system matrices with relatively few quadrature points. For $n_G = 11$ the error in all examples is already below 10^{-10} , which is why we set $n_G = 11$ for all subsequent experiments.

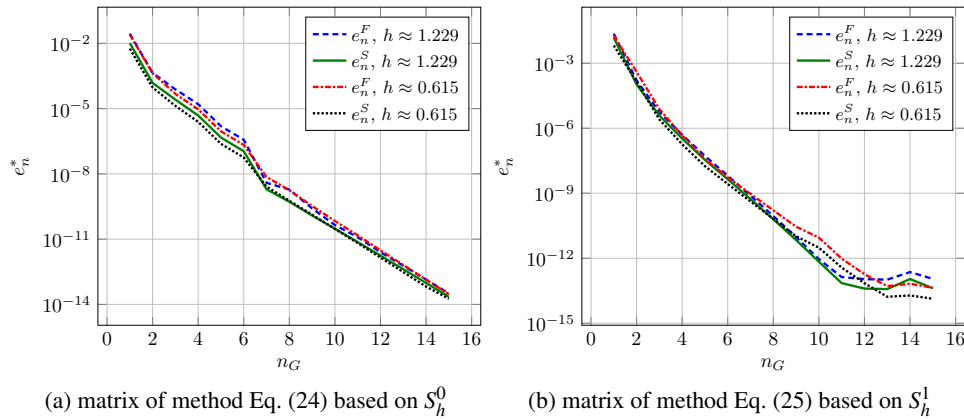


Figure 5: Accuracy of system matrices for varying orders of quadrature.

4.2.2 Convergence study on a cube

Let $\Omega^- = (-\frac{1}{2}, \frac{1}{2})^3$ be the unit cube. In order to study the effect of the simulation end time several values of T are considered. To measure the error, the difference of u and SLw_h is examined, where w_h is the solution of Eq. (24) or Eq. (25). In particular, we compute

$$e_h^Q = \frac{\sum_{i=1}^m |u(T, x_i) - SLw_h(T, x_i)|}{\sum_{i=1}^m |u(T, x_i)|}$$

for $m = 488$ points $x_i \in \Omega^+$ spaced equally on the boundary of the cube $(-\frac{3}{5}, \frac{3}{5})^3$. The convergence study is depicted in Section 4.2.2. On the one hand, it can be observed that for sufficiently small T both methods seem to converge (roughly) linearly with respect to the mesh size h . On the other hand, for $T \geq 3$ approach Eq. (25) fails to converge at all. Although method Eq. (24) seems to converge in the examined case it yields considerable errors for $T = 5$. Moreover, we conducted the same study on a different mesh and procedure Eq. (24) failed similarly to method Eq. (25) in the presented test. This might indicate that these methods are not stable for arbitrary values of T . It is well-known that certain bilinear forms of RPBEs are positive definite iff T is sufficiently small, see [36]. For the unit cube $T < 1$ is sufficient for positive definiteness as stated in [36, Prop. 3.4.]. Nevertheless, the “naive” collocation approaches Eqs. (24) and (25) are expected to tend more towards instability than the variational formulations employed in the cited reference. To the best of our knowledge, no theoretical results for collocation methods for RPBEs on polyhedral boundaries are available (especially in the context of space-time meshes as used in this work).

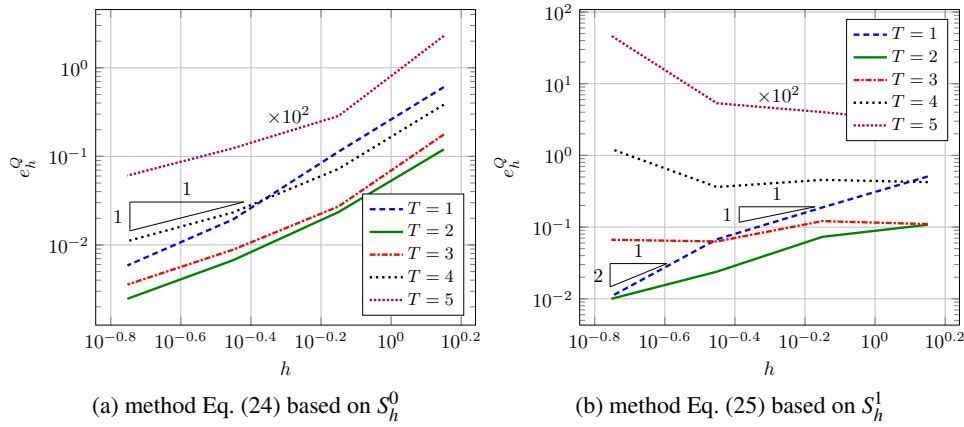


Figure 6: Convergence study of the collocation methods for a sequence of uniform meshes of the unit cube. Since the errors for $T = 5$ are extraordinarily large they are multiplied by 10^{-2} .

4.2.3 Convergence study on a sphere

In case Ω^- is the unit sphere, the density w satisfying Eq. (7) is known for certain right hand sides g , see [62]. We choose

$$g(t,x) = \begin{cases} t^4 \exp(-2t) & t > 0 \\ 0 & t \leq 0 \end{cases} \quad \text{for } (t,x) \in \Sigma$$

which is constant with respect to the spatial component. The corresponding density w follows from [62, Eq. 4.11]. Both collocation approaches Eqs. (24) and (25) are used to obtain approximations w_h for a sequence of quasi-uniform meshes. Again, each mesh Σ_N is a polyhedral approximation of the surface of the unit sphere. The error

$$e_h^\Sigma = \frac{\|w - w_h\|_{L^2(\Sigma_N)}}{\|w\|_{L^2(\Sigma_N)}}$$

is shown in Section 4.2.3. We see that method Eq. (24) converges linearly, while approach Eq. (25) converges quadratically in h for all examined simulation end times. Note that for this scenario [36, Prop. 3.4.] implies that $T < 2$ is sufficient for positive definiteness of a bilinear form associated to Eq. (7). The fact that the methods converge in all investigated cases suggests that the smoothness of the domain plays a crucial role when it comes to the stability of standard collocation schemes.

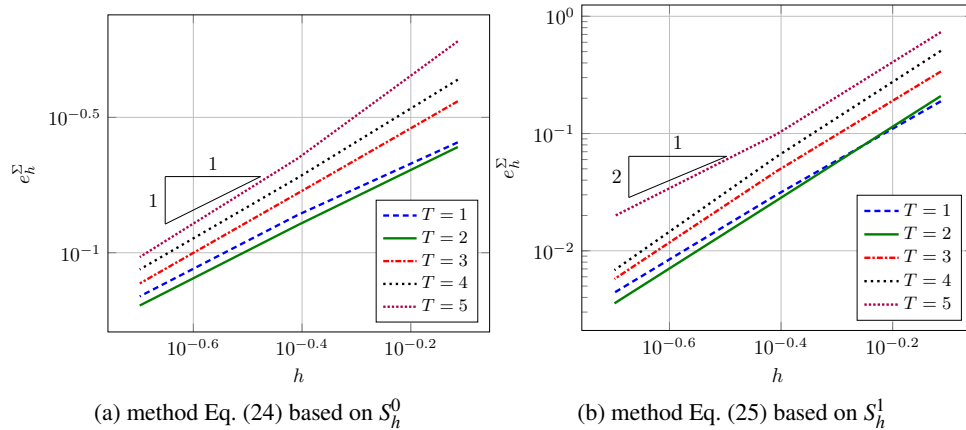


Figure 7: Convergence study of the collocation methods for a sequence of meshes of the unit sphere.

4.3 Comparison to a classical approach

The experiments of Section 4.2 show that the proposed space-time collocation methods do not necessarily converge. To put this observation into perspective we shall compare the space-time method to a classical approach based on semi-discretization. The employed method is based on

a decomposition of Γ into a mesh Γ_h consisting of triangular elements. We denote the lengths of the longest and shortest edge by h and h_{\min} respectively. The interval $[0, T]$ is partitioned into $m \in \mathbb{N}$ time steps of constant size $\Delta t = T/m$. We use continuous piecewise linear basis functions (hat functions) in both space and time, i.e. the trial space is the product $S_{\Delta t}^1(0, T) \times S_h^1(\Gamma_h)$. To obtain approximations of Eq. (7) the equation is collocated at the time steps $\{i\Delta t\}_{i=1}^m$ and the vertices of the mesh Γ_h . This procedure can already be found in [47] for two spatial dimensions. The method ‘‘S1T1’’ in [13], which is analyzed for flat Γ , is also quite similar to the described approach. Finally, the retarded single layer operator is computed accurately by use of polar coordinates [28] and a quadrature rule with 11 integration points.

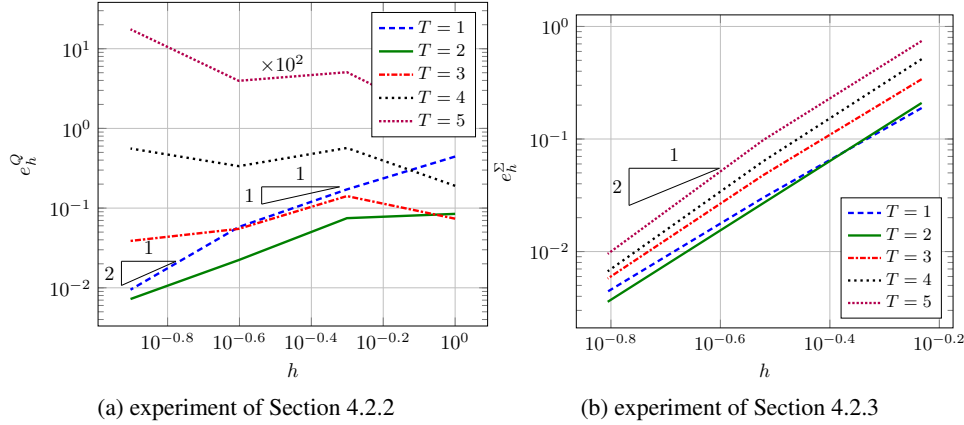


Figure 8: Convergence study of a classical method based on $S_{\Delta t}^1(0, T) \times S_h^1(\Gamma_h)$ for the unit cube (left, $\Delta t = h = \sqrt{2}h_{\min}$) and the unit sphere (right, $\Delta t \approx 0.85h \approx 1.41h_{\min}$).

Since we compare this classical method to the space-time method Eq. (25) based on $S_h^1(\Sigma_N)$ the meshes are chosen such that the number of degrees of freedom coincides for both approaches. The results for the experiments of Sections 4.2.2 and 4.2.3 are shown in Figs. 8a and 8b respectively, which resemble the results of the space-time procedure remarkably. On the one hand, comparing Fig. 8a to Fig. 6b we observe that the classical method seems to fail in a similar fashion as our space-time approach. On the other hand, Fig. 8b shows that the classical method converges immaculately for the spherical domain, according with the results of Fig. 7b.

To conclude this section, we endow the following interpretation to the findings of the presented experiments: Discretization schemes for RPBEs based on unstructured space-time meshes are technically feasible and the obtained numerical results indicate their great potential. Having said that, the discussed space-time collocation methods appear to have similar stability issues as classical approaches. The success of the space-time methodology hinges on finding stable formulations in general settings.

5 Concluding remarks

In this paper, a space-time boundary element method for the wave equation in $3 + 1$ dimensions is proposed. Its key feature are basis functions that do not distinguish between space and time

coordinates but are based on unstructured meshes of the lateral boundary of the space-time cylinder. An explicit representation of retarded potential integral operators which genuinely conforms to the space-time setting is derived and a numerical integration scheme is developed. Numerical experiments confirm that space-time discretization schemes for integral equations of hyperbolic problems are technically feasible and can yield promising results. However, the stability of the underlying collocation schemes is open. Numerical tests indicate that the proposed space-time collocation methods encounter similar stability issues as classical schemes. Further research is necessary to reveal correct formulations.

The major drawback of the presented approach is its increased demand in terms of computational resources compared to classical methods. This issue might spark further research on space-time discretization schemes. On the one hand, the proposed quadrature technique as well as its implementation could be improved. On the other hand, the development of fast methods, well-established in boundary element methods for elliptic problems, is a topic of research that seems to present itself.

Ultimately, one might consider the collocation method discussed in this work as a precursor to more involved Galerkin discretizations. However, their favourable properties in terms of stability come at the price of more intricate integrals in the computation of the Galerkin matrix entries. Nevertheless, our work presents a strong indication that space-time discretizations of boundary integral equations of hyperbolic problems have great potential.

A Proofs of the lemmas

Proof of Lemma 3.1. By the chain rule $\nabla(\phi \circ \chi_\tau(\xi)) = J_\tau^\top(\xi) \nabla \phi \circ \chi_\tau(\xi)$ holds when ϕ is differentiable at $\chi_\tau(\xi)$. Since ϕ is Lipschitz continuous it is differentiable almost everywhere by Rademacher's theorem, in particular for $(\zeta, y) = \chi_\tau(\xi)$ it holds

$$\nabla \phi(\zeta, y) = \left[\begin{array}{c} 1 \\ -\frac{x-y}{\|x-y\|} \end{array} \right], \quad \|\nabla \phi(\zeta, y)\|^2 = 2$$

when $x \neq y$. For simplicity of notation we set $q := \nabla \phi(\zeta, y)$ and omit the argument lists as well as the subscript τ . Let $z := q - \langle q, v \rangle v$ where $\text{span}\{v\} = \ker J^\top$ and $\|v\| = 1$. It holds $\|z\|^2 = \|q\|^2 - \langle q, v \rangle^2 = 2 - \langle q, v \rangle^2$. From $v^\top = (0 \quad n^\top)$ and the Cauchy-Schwarz inequality $|\langle q, v \rangle| = \|x-y\|^{-1} |\langle x-y, n \rangle| \leq 1$ follows. We conclude

$$\|z\|^2 = 2 - \langle q, v \rangle^2 \geq 1. \quad (28)$$

Let $\beta_1 = 0 < \beta_2 \leq \beta_3 \leq \beta_4$ be the eigenvalues of the (symmetric) matrix JJ^\top . This enables the decomposition $JJ^\top = VCV^\top$ with $C := \text{diag}(\beta_i)_{i=1}^4$ and $V^\top = V^{-1}$ contains the normalized eigenvectors $\{v, e_2, e_3, e_4\}$. Since $q - z = \langle q, v \rangle v \in \ker J^\top$ it holds $CV^\top(q - z) = 0$ and we obtain

$$\begin{aligned} \|J^\top q\|^2 &= \langle JJ^\top q, q \rangle = \langle CV^\top q, V^\top q \rangle \\ &= \langle CV^\top z, V^\top q \rangle = \langle V^\top z, CV^\top q \rangle = \langle CV^\top z, V^\top z \rangle. \end{aligned}$$

Using the basis spanned by the eigenvectors in conjunction with Eq. (28) the lower bound

$$\|J^\top q\|^2 = \langle CV^\top z, V^\top z \rangle = \sum_{i=2}^4 \beta_i \langle z, e_i \rangle^2 \geq \beta_2 \sum_{i=2}^4 \langle z, e_i \rangle^2 = \beta_2 \|z\|^2 \geq \beta_2$$

follows, where the last equality is due to $\|z\|^2 = \sum_{i=2}^4 \langle z, e_i \rangle^2 + \langle z, v \rangle^2$ and $\langle z, v \rangle = 0$. The upper bound is due to the operator norm $\|J^\top q\|^2 \leq \|J^\top\|^2 \|q\|^2 = 2\beta_4$. \square

Proof of Lemma 3.2. The matrix A is of the form $A = J^\top J - 2j_t j_t^\top$ with $j_t \in \mathbb{R}^3$. From $\text{rank } J = 3$ it follows that $J^\top J$ is positive definite, hence A can have at most one non-positive eigenvalue [31, p. 325], implying $0 < \lambda_2 \leq \lambda_3$. We have

$$\lambda_1 < 0 \Leftrightarrow \exists x \in \mathbb{R}^3 : \langle Ax, x \rangle = \langle MJx, Jx \rangle < 0 \Leftrightarrow \exists y \in \text{ran } J : \langle My, y \rangle < 0.$$

The vector $y \in \mathbb{R}^4$ is in $\text{ran } J$ iff $0 = \langle y, v \rangle = y_t v_t + \langle y_x, v_x \rangle$, since $\ker J^\top = \text{span}\{v\}$. Using $v_t = 0$ it follows

$$\lambda_1 < 0 \Leftrightarrow \exists y \in \mathbb{R}^4 : \langle y_x, v_x \rangle = 0 \wedge \langle My, y \rangle = \|y_x\|^2 - y_t^2 < 0.$$

Choosing $y = (\alpha, 0, 0, 0)^\top$, i.e. $y_t = \alpha \in \mathbb{R} \setminus \{0\}$ and $y_x = 0$ satisfies above condition. This proves $\lambda_1 < 0$ and the invertibility of A . Consequently, ξ_0 is the unique solution of $A\xi_0 = -b$ or by using $A = J^\top MJ$ and $b = -J^\top Mz_0$

$$J^\top MJ\xi_0 = J^\top Mz_0 \Leftrightarrow J^\top M(J\xi_0 - z_0) = 0.$$

It follows $M(J\xi_0 - z_0) \in \ker J^\top$ or equivalently

$$\exists \beta \in \mathbb{R} : J\xi_0 - z_0 = \beta Mv \Leftrightarrow J\xi_0 = z_0 + \beta Mv \quad (29)$$

where we used $M = M^{-1}$. A solution to Eq. (29) exists iff the right hand side $z_0 + \beta Mv$ is orthogonal to $\ker J^\top$. Since the solution of Eq. (29) is equivalent to the unique solution of $A\xi_0 = -b$ the condition $\langle z_0 + \beta Mv, v \rangle = 0$ must hold and from $\langle Mv, v \rangle = 1$ follows $\beta = -\langle z_0, v \rangle$. Insertion into $c_M = c_0 + \langle b, \xi_0 \rangle$ with $c_0 = \langle Mz_0, z_0 \rangle$ yields

$$c_M = \langle Mz_0, z_0 \rangle - \langle J^\top Mz_0, \xi_0 \rangle = \langle Mz_0, z_0 - J\xi_0 \rangle = -\beta \langle Mz_0, Mv \rangle = \langle z_0, v \rangle^2$$

which proves the assertion. \square

Proof of Lemma 3.3. For any $\rho \in \text{dom } \psi$ the transformation determinant reads

$$g_\psi(\rho) = \left(\|\partial_1 \psi(\rho)\|^2 \|\partial_2 \psi(\rho)\|^2 - \langle \partial_1 \psi(\rho), \partial_2 \psi(\rho) \rangle^2 \right)^{1/2}.$$

Set $X = C$ for $c_M = 0$ or $X = H$ for $c_M > 0$. The chain rule in conjunction with the orthogonality of the eigenvectors of A , i.e. $E^\top = E^{-1}$ yields

$$\langle \partial_i \psi(\rho), \partial_j \psi(\rho) \rangle = \langle E \partial_i \psi_X(\rho), E \partial_j \psi_X(\rho) \rangle = \langle \partial_i \psi_X(\rho), \partial_j \psi_X(\rho) \rangle, \quad i, j = 1, 2.$$

The asserted representations of g_ψ follow by computing the partial derivatives of ψ_C and ψ_H respectively with

$$\begin{aligned} g_C(\rho) &= \left[\left(\frac{\sin^2 \rho_1}{\lambda_2} + \frac{\cos^2 \rho_1}{\lambda_3} \right) \left(\frac{1}{-\lambda_1} + \frac{\cos^2 \rho_1}{\lambda_2} + \frac{\sin^2 \rho_1}{\lambda_3} \right) - \frac{(\lambda_3 - \lambda_2)^2}{\lambda_2^2 \lambda_3^2} \sin^2 \rho_1 \cos^2 \rho_1 \right]^{1/2} \\ &= \left[\frac{1}{-\lambda_1} \left(\frac{\sin^2 \rho_1}{\lambda_2} + \frac{\cos^2 \rho_1}{\lambda_3} \right) + \frac{1}{\lambda_2 \lambda_3} \right]^{1/2}, \\ g_H(\rho) &= \left[\left(\frac{\sin^2 \rho_1}{\lambda_2} + \frac{\cos^2 \rho_1}{\lambda_3} \right) \left(\frac{\tanh^2 \rho_2}{-\lambda_1} + \frac{\cos^2 \rho_1}{\lambda_2} + \frac{\sin^2 \rho_1}{\lambda_3} \right) - \frac{(\lambda_3 - \lambda_2)^2}{\lambda_2^2 \lambda_3^2} \sin^2 \rho_1 \cos^2 \rho_1 \right]^{1/2} \\ &= \left[\frac{\tanh^2 \rho_2}{-\lambda_1} \left(\frac{\sin^2 \rho_1}{\lambda_2} + \frac{\cos^2 \rho_1}{\lambda_3} \right) + \frac{1}{\lambda_2 \lambda_3} \right]^{1/2}. \end{aligned}$$

As we direct our attention towards the second part of the theorem set

$$\eta := \psi_X(\rho), \quad \xi := \kappa(\eta) = \kappa \circ \psi_X(\rho), \quad \begin{pmatrix} \zeta \\ y \end{pmatrix} := \begin{pmatrix} |_t \chi(\xi) \\ |_x \chi(\xi) \end{pmatrix} = \chi(\xi) = \chi \circ \kappa \circ \psi_X(\rho).$$

Using $(\zeta, y) \in \Xi$ and the explicit representations of the affine maps χ and κ it follows

$$d_x(y) = \|x - y\| = t - \zeta = t - t_0 - j_t^\top \xi = t - t_0 - j_t^\top \xi_O - j_t^\top E \eta.$$

By Eq. (29) there exists a $\beta \in \mathbb{R}$ such that $t - t_0 - j_t^\top \xi_O = \beta v_t$. From $v_t = 0$ it follows $d_x(y) = -j_t^\top E \eta = -\sum_{i=1}^3 \langle j_t, e_i \rangle \eta_i$. Insertion of $\eta = \psi_C(\rho)$ for $c_M = 0$ and $\eta = \psi_H(\rho)$ for $c_M > 0$ yields the asserted representations with

$$\begin{aligned} f_C(\rho) &= -\frac{\langle e_1, j_t \rangle}{\sqrt{-\lambda_1}} - \frac{\langle e_2, j_t \rangle}{\sqrt{\lambda_2}} \cos \rho_1 - \frac{\langle e_3, j_t \rangle}{\sqrt{\lambda_3}} \sin \rho_1, \\ f_H(\rho) &= -\frac{\langle e_1, j_t \rangle}{\sqrt{-\lambda_1}} - \tanh \rho_2 \left(\frac{\langle e_2, j_t \rangle}{\sqrt{\lambda_2}} \cos \rho_1 + \frac{\langle e_3, j_t \rangle}{\sqrt{\lambda_3}} \sin \rho_1 \right). \end{aligned}$$

Using $\min_{x \in \mathbb{R}} \left(-\frac{\langle e_2, j_t \rangle}{\sqrt{\lambda_2}} \cos x - \frac{\langle e_3, j_t \rangle}{\sqrt{\lambda_3}} \sin x \right) = -\left(\frac{\langle e_2, j_t \rangle^2}{\lambda_2} + \frac{\langle e_3, j_t \rangle^2}{\lambda_3} \right)^{1/2}$ we obtain

$$f_X(\rho) \geq -\frac{\langle e_1, j_t \rangle}{\sqrt{-\lambda_1}} - \left(\frac{\langle e_2, j_t \rangle^2}{\lambda_2} + \frac{\langle e_3, j_t \rangle^2}{\lambda_3} \right)^{1/2}. \quad (30)$$

The matrix A can be rewritten $A = J_x^\top J_x - j_t j_t^\top$ with $\dim \ker J_x = 1$. Let $v \in \ker J_x$ be such that $\langle v, j_t \rangle = -1$. Note that v exists, since $j_t \perp \ker J_x$ would imply $\ker A \neq \{0\}$ which contradicts Lemma 3.2. Moreover, $Av = J_x^\top J_x v - \langle v, j_t \rangle j_t = j_t$, i.e. v is the unique solution of $Av = j_t$. With the diagonalization $A = EDE^\top$ we obtain

$$-1 = \langle v, j_t \rangle = \langle A^{-1} j_t, j_t \rangle = \left\langle D^{-1} E^\top j_t, E^\top j_t \right\rangle = \sum_{i=1}^3 \frac{\langle e_i, j_t \rangle^2}{\lambda_i}$$

and $\frac{\langle e_1, j_t \rangle^2}{-\lambda_1} = 1 + \sum_{i=2}^3 \frac{\langle e_i, j_t \rangle^2}{\lambda_i}$. From estimate Eq. (30) in conjunction with $\langle e_1, j_t \rangle < 0$

$$f_X(\rho) \geq \left(1 + \frac{\langle e_2, j_t \rangle^2}{\lambda_2} + \frac{\langle e_3, j_t \rangle^2}{\lambda_3} \right)^{1/2} - \left(\frac{\langle e_2, j_t \rangle^2}{\lambda_2} + \frac{\langle e_3, j_t \rangle^2}{\lambda_3} \right)^{1/2} > 0$$

follows, which completes the proof. \square

B Construction of Λ_1

A crucial component of the integration scheme proposed in Section 3.4 is a first-order approximation Λ_1 sufficiently close to $\Lambda = \psi^{-1}(\partial \hat{\tau} \cap \text{ran } \psi)$. Let $\mathcal{F} = \{f_i\}_{i=1}^4$ be the set of four triangular faces of the reference tetrahedron $\hat{\tau}$, then

$$\partial \hat{\tau} \cap \text{ran } \psi = \bigcup_{f \in \mathcal{F}} f \cap \text{ran } \psi.$$

Moreover, let $P_f \supset f$ be the plane in which $f \in \mathcal{F}$ lies. As discussed in Section 3.3 $\text{ran } \psi$ is either a cone or one sheet of a two-sheeted hyperboloid. Consequently, $P_f \cap \text{ran } \psi$ is a planar section through a cone/hyperboloid and a bijective parametrization $\omega_f : \text{dom } \omega_f \rightarrow P_f \cap \text{ran } \psi$ with $\text{dom } \omega_f \subseteq \mathbb{R}$ is available. The set $I_f = \omega_f^{-1}(f \cap \text{ran } \psi)$ is obtained via following procedure. Let $\{r_i\}_{i=1}^{n_f} = \omega_f^{-1}(\partial f \cap \text{ran } \psi)$ be the set of parameter points where the boundary of the triangle f (composed of three lines) intersects the quadric $\text{ran } \psi$. Assume that $r_i < r_{i+1}, i = 1, \dots, n_f - 1$, then

$$I_f = \bigcup_{i=1, \dots, n_f-1: \omega_f(\frac{1}{2}(r_i+r_{i+1})) \in f} (r_i, r_{i+1}). \quad (31)$$

Note that, since ∂f is composed of line segments, computing $\partial f \cap \text{ran } \psi$ amounts to solving quadratic equations in one variable.

Our goal is to employ the parametrization ω_f to build the line elements of Λ_1 . To this end, consider the set of start points $\{s_i^A\}_{i=1}^{m_f}$ and end points $\{s_i^B\}_{i=1}^{m_f}$ such that

$$\bar{I}_f = \bigcup_{i=1}^{m_f} [s_i^A, s_i^B]$$

with the number of segments $m_f \in \mathbb{N}$. These points are due to a uniform partitioning of the intervals in Eq. (31). The set of line elements $\Lambda_1^f = \{\sigma_i\}_{i=1}^{m_f}$ is obtained via

$$\text{dom } \psi \ni \rho_{\sigma_i}^* = \psi^{-1} \circ \omega_f(s_i^*), \quad i = 1, \dots, m_f, * \in \{A, B\}$$

and using $\rho_{\sigma_i}^A$ as start points and $\rho_{\sigma_i}^B$ as end points. As already indicated, each line element has to be sufficiently close to Λ . To quantify proximity, we use the condition

$$\text{diam } \sigma_i \leq c_K \inf_{s \in (s_i^A, s_i^B)} \frac{1}{|\kappa_\Lambda(\psi^{-1} \circ \omega_f(s))|} \quad (32)$$

where $\kappa_\Lambda(\rho)$ is the curvature of Λ at $\rho \in \Lambda$ and $c_K \in (0, 1)$. If σ_i does not satisfy Eq. (32) it is refined by adding the point $\frac{1}{2}(s_i^A + s_i^B)$ to the list of start and end points, until the criterion is met. In our implementation the infimum in Eq. (32) is not computed exactly, but the minimum of a fixed number of equally spaced sampling points is used. To compensate this, we use $c_K = 1/2$ in all of the conducted tests. Finally, the set Λ_1 is obtained by collecting the line elements of each face, i.e. $\Lambda_1 = \bigcup_{f \in \mathcal{F}} \Lambda_1^f$.

Acknowledgments

We greatly appreciate the discussions with M.H. Gfrerer, G. Of, and M. Zank. Our exchanges shaped several ideas uttered in this publication.

References

- [1] A. Aimi, M. Diligenti, A. Frangi, and C. Guardasoni. A stable 3d energetic galerkin bem approach for wave propagation interior problems. *Eng. Anal. Bound. Elem.*, 36(12):1756–1765, 2012. doi: 10.1016/j.enganabound.2012.06.003.
- [2] A. Aimi, M. Diligenti, A. Frangi, and C. Guardasoni. Neumann exterior wave propagation problems: computational aspects of 3d energetic galerkin bem. *Comput. Mech.*, 51(4): 475–493, 2013. doi: 10.1007/s00466-012-0796-5.
- [3] J. Ballani, L. Banjai, S. Sauter, and A. Veit. Numerical solution of exterior maxwell problems by galerkin bem and runge-kutta convolution quadrature. *Numer. Math.*, 123(4): 643–670, 2013. doi: 10.1007/s00211-012-0503-7.
- [4] A. Bamberger and T. Ha Duong. Formulation variationnelle espace-temps pour le calcul par potentiel retardé de la diffraction d’une onde acoustique (i). *Math. Methods Appl. Sci.*, 8(1):405–435, 1986. doi: doi:10.1002/mma.1670080127.
- [5] A. Bamberger and T. Ha Duong. Formulation variationnelle pour le calcul de la diffraction d’une onde acoustique par une surface rigide. *Math. Methods Appl. Sci.*, 8(4):598–608, 1986. doi: 10.1002/mma.1670080139.
- [6] L. Banjai and S. Sauter. Rapid solution of the wave equation in unbounded domains. *SIAM J. Numer. Anal.*, 47(1):227–249, 2009. doi: 10.1137/070690754.
- [7] L. Banjai and M. Schanz. Wave propagation problems treated with convolution quadrature and bem. In U. Langer, M. Schanz, O. Steinbach, and W.L. Wendland, editors, *Fast Boundary Element Methods in Engineering and Industrial Applications*, pages 145–184. Springer Berlin Heidelberg, Berlin, Heidelberg, 2012. ISBN 978-3-642-25670-7. doi: 10.1007/978-3-642-25670-7_5.
- [8] L. Banz, H. Gimperlein, Z. Nezhi, and E.P. Stephan. Time domain bem for sound radiation of tires. *Comput. Mech.*, 58(1):45–57, 2016. doi: 10.1007/s00466-016-1281-3.
- [9] M. Behr. Simplex space-time meshes in finite element simulations. *Internat. J. Numer. Methods Fluids*, 57(9):1421–1434, 2008. doi: 10.1002/fld.1796.
- [10] B. Birgisson, E. Siebrits, and A.P. Peirce. Elastodynamic direct boundary element methods with enhanced numerical stability properties. *Internat. J. Numer. Methods Engrg.*, 46(6): 871–888, 1999. doi: 10.1002/(SICI)1097-0207(19991030)46:6<871::AID-NME698>3.0.CO;2-6.
- [11] M.J. Bluck and S.P. Walker. Analysis of three-dimensional transient acoustic wave propagation using the boundary integral equation method. *Internat. J. Numer. Methods Engrg.*, 39(8):1419–1431, 1996. doi: 10.1002/(SICI)1097-0207(19960430)39:8<1419::AID-NME911>3.0.CO;2-C.

- [12] M. Costabel and F.-J. Sayas. Time-dependent problems with the boundary integral equation method. *Encycl. Comput. Mech. Second Ed.*, 2:1–24, 2017. doi: 10.1002/9781119176817.ecm2022.
- [13] P. Davies and D. Duncan. Stability and convergence of collocation schemes for retarded potential integral equations. *SIAM J. Numer. Anal.*, 42(3):1167–1188, 2004. doi: 10.1137/S0036142901395321.
- [14] P.J. Davies. A stability analysis of a time marching scheme for the general surface electric field integral equation. *Appl. Numer. Math.*, 27(1):33–57, 1998. doi: 10.1016/S0168-9274(97)00107-4.
- [15] P.J. Davies and D.B. Duncan. Averaging techniques for time-marching schemes for retarded potential integral equations. *Appl. Numer. Math.*, 23(3):291–310, 1997. doi: 10.1016/S0168-9274(96)00069-4.
- [16] L. Demkowicz, J. Gopalakrishnan, S. Nagaraj, and P. Sepúlveda. A spacetime dpg method for the schrödinger equation. *SIAM J. Numer. Anal.*, 55(4):1740–1759, 2017. doi: 10.1137/16M1099765.
- [17] A. Demlow and G. Dziuk. An adaptive finite element method for the laplace-beltrami operator on implicitly defined surfaces. *SIAM J. Numer. Anal.*, 45(1):421–442, 2007. doi: 10.1137/050642873.
- [18] W. Dörfler, S. Findeisen, and C. Wieners. Space-time discontinuous galerkin discretizations for linear first-order hyperbolic evolution systems. *Comput. Methods Appl. Math.*, 16(3):409–428, 2016. doi: 10.1515/cmam-2016-0015.
- [19] H. Federer. Curvature measures. *Trans. Amer. Math. Soc.*, 93(3):418–491, 1959. doi: 10.1090/S0002-9947-1959-0110078-1.
- [20] P. Foteinos and N. Chrisochoides. 4d space-time delaunay meshing for medical images. *Eng. Comput.*, 31(3):499–511, 2015. ISSN 1435-5663. doi: 10.1007/s00366-014-0380-z.
- [21] A. Frangi. “causal” shape functions in the time domain boundary element method. *Comput. Mech.*, 25(6):533–541, Jun 2000. ISSN 1432-0924. doi: 10.1007/s004660050501.
- [22] M.B. Friedman and R. Shaw. Diffraction of pulses by cylindrical obstacles of arbitrary cross section. *J. Appl. Mech.*, 29(1):40–46, 1962. doi: 10.1115/1.3636495.
- [23] T.-P. Fries and S. Omerović. Higher-order accurate integration of implicit geometries. *Internat. J. Numer. Methods Engrg.*, 106(5):323–371, 2016. doi: 10.1002/nme.5121.
- [24] T.P. Fries, Omerović, D. Schöllhammer, and J. Steidl. Higher-order meshing of implicit geometries-part i: Integration and interpolation in cut elements. *Comput. Methods Appl. Mech. Engrg.*, 313:759–784, 2017. doi: 10.1016/j.cma.2016.10.019.

- [25] M. Gander and M. Neumüller. Analysis of a new space-time parallel multigrid algorithm for parabolic problems. *SIAM J. Sci. Comput.*, 38(4):A2173–A2208, 2016. doi: 10.1137/15M1046605.
- [26] M.H. Gfrerer and M. Schanz. A high-order fem with exact geometry description for the laplacian on implicitly defined surfaces. *Internat. J. Numer. Methods Engrg.*, 114(11):1163–1178, 2018. doi: 10.1002/nme.5779.
- [27] H. Gimperlein and D. Stark. Algorithmic aspects of enriched time domain boundary element methods. *Eng. Anal. Bound. Elem.*, 2018. doi: 10.1016/j.enganabound.2018.02.010. Article in Press.
- [28] H. Gimperlein, M. Maischak, and E.P. Stephan. Adaptive time domain boundary element methods with engineering applications. *J. Integral Equations Appl.*, 29(1):75–105, 2017. doi: 10.1216/JIE-2017-29-1-75.
- [29] H. Gimperlein, F. Meyer, C. Özdemir, D. Stark, and E.P. Stephan. Boundary elements with mesh refinements for the wave equation. *Numer. Math.*, 139(4):867–912, 2018. doi: 10.1007/s00211-018-0954-6.
- [30] M. Gläfke. *Adaptive Methods for Time Domain Boundary Integral Equations*. PhD thesis, Brunel University London, 2012.
- [31] G. Golub. Some modified matrix eigenvalue problems. *SIAM Rev.*, 15(2):318–334, 1973. doi: 10.1137/1015032.
- [32] J. Gopalakrishnan and P. Sepúlveda. A spacetime dpg method for the wave equation in multiple dimensions, 2017.
- [33] J. Gopalakrishnan, J. Schöberl, and C. Wintersteiger. Mapped tent pitching schemes for hyperbolic systems. *SIAM J. Sci. Comput.*, 39(6):B1043–B1063, 2017. doi: 10.1137/16M1101374.
- [34] T. Ha-Duong. On retarded potential boundary integral equations and their discretisation. In M. Ainsworth, P. Davies, D. Duncan, B. Rynne, and P. Martin, editors, *Topics in Computational Wave Propagation*, volume 31, pages 301–336. Springer Berlin Heidelberg, Berlin, Heidelberg, 2003. doi: 10.1007/978-3-642-55483-4_8.
- [35] G.M. Hulbert and T.J.R. Hughes. Space-time finite element methods for second-order hyperbolic equations. *Comput. Methods Appl. Mech. Engrg.*, 84(3):327–348, 1990. doi: 10.1016/0045-7825(90)90082-W.
- [36] P. Joly and J. Rodríguez. Mathematical aspects of variational boundary integral equations for time dependent wave propagation. *J. Integral Equations Appl.*, 29(1):137–187, 2017. doi: 10.1216/JIE-2017-29-1-137.
- [37] E. Karabelas and M. Neumüller. Generating admissible space-time meshes for moving domains in $d + 1$ -dimensions, 2015.

- [38] L. Kudela, N. Zander, T. Bog, S. Kollmannsberger, and E. Rank. Efficient and accurate numerical quadrature for immersed boundary methods. *Adv. Model. and Simul. in Eng. Sci.*, 2(1):10, 2015. ISSN 2213-7467. doi: 10.1186/s40323-015-0031-y.
- [39] C. Lehrenfeld. High order unfitted finite element methods on level set domains using isoparametric mappings. *Comput. Methods Appl. Mech. Engrg.*, 300:716–733, 2016. doi: 10.1016/j.cma.2015.12.005.
- [40] M. Lopez-Fernandez and S. Sauter. Generalized convolution quadrature with variable time stepping. *IMA J. Numer. Anal.*, 33(4):1156–1175, 2013. doi: 10.1093/imanum/drs034.
- [41] M. Lopez-Fernandez and S. Sauter. Generalized convolution quadrature with variable time stepping. part ii: Algorithm and numerical results. *Appl. Numer. Math.*, 94:88–105, 2015. doi: 10.1016/j.apnum.2015.03.004.
- [42] M. Lopez-Fernandez and S. Sauter. Generalized convolution quadrature based on runge-kutta methods. *Numer. Math.*, 133(4):743–779, 2016. doi: 10.1007/s00211-015-0761-2.
- [43] C. Lubich. Convolution quadrature and discretized operational calculus. i. *Numer. Math.*, 52(2):129–145, 1988. doi: 10.1007/BF01398686.
- [44] C. Lubich. Convolution quadrature and discretized operational calculus. ii. *Numer. Math.*, 52(4):413–425, 1988. doi: 10.1007/BF01462237.
- [45] C. Lubich. On the multistep time discretization of linear initial-boundary value problems and their boundary integral equations. *Numer. Math.*, 67(3):365–389, 1994. doi: 10.1007/s002110050033.
- [46] N. Manson and J. Tausch. Quadrature for parabolic galerkin bem with moving surfaces. *Comput. Math. Appl.*, 77(1):1–14, 2019. doi: 10.1016/j.camwa.2018.09.004.
- [47] Webe João Mansur. *A time-stepping technique to solve wave propagation problems using the boundary element method*. PhD thesis, University of Southampton, 1983.
- [48] W.J. Mansur and C.A. Brebbia. Numerical implementation of the boundary element method for two dimensional transient scalar wave propagation problems. *Appl. Math. Model.*, 6(4):299–306, 1982. doi: 10.1016/S0307-904X(82)80038-3.
- [49] B. Müller, F. Kummer, and M. Oberlack. Highly accurate surface and volume integration on implicit domains by means of moment-fitting. *Internat. J. Numer. Methods Engrg.*, 96(8):512–528, 2013. doi: 10.1002/nme.4569.
- [50] M. Neumüller. *Space-Time Methods: Fast Solvers and Applications*. PhD thesis, Graz University of Technology, 2013.
- [51] M. Neumüller, P.S. Vassilevski, and U.E. Villa. Space-time cfoals methods with amge upscaling. In C.-O. Lee, X.-C. Cai, D.E. Keyes, H.H. Kim, A. Klawonn, E.-J. Park, and O.B. Widlund, editors, *Domain Decomposition Methods in Science and Engineering XXIII*,

- volume 116, pages 253–260, Cham, 2017. Springer International Publishing. doi: 10.1007/978-3-319-52389-7_25.
- [52] N. Ortner. Regularisierte faltung von distributionen. teil 2: Eine tabelle von fundamental-lösungen. *Z. Angew. Math. Phys.*, 31(1):155–173, 1980. doi: 10.1007/BF01601710.
- [53] N. Ortner and P. Wagner. *Fundamental Solutions of Linear Partial Differential Operators: Theory and Practice*. Springer, Cham, 2015. doi: 10.1007/978-3-319-20140-5.
- [54] D. Pölz, M.H. Gfrerer, and M. Schanz. Wave propagation in elastic trusses: An approach via retarded potentials. *Wave Motion*, 87:37–57, 2019. doi: 10.1016/j.wavemoti.2018.06.002.
- [55] W.H. Press, S.A. Teukolsky, W.T. Vetterling, and B.P. Flannery. *Numerical Recipes: The Art of Scientific Computing*. Cambridge University Press, Cambridge, UK, 3 edition, 2007.
- [56] E. Rothe. Zweidimensionale parabolische randwertaufgaben als grenzfall eindimensionaler randwertaufgaben. *Math. Ann.*, 102(1):650–670, 1930. doi: 10.1007/BF01782368.
- [57] B.P. Rynne. Instabilities in time marching methods for scattering problems. *Electromagnetics*, 6(2):129–144, 1986. doi: 10.1080/02726348608915207.
- [58] B.P. Rynne. Time domain scattering from arbitrary surfaces using the electric field integral equation. *J. Electromagn. Waves Appl.*, 5(1):93–112, 1991. doi: 10.1163/156939391X00491.
- [59] B.P. Rynne. The well-posedness of the electric field integral equation for transient scattering from a perfectly conducting body. *Math. Methods Appl. Sci.*, 22(7):619–631, 1999. doi: 10.1002/(SICI)1099-1476(19990510)22:7<619::AID-MMA59>3.0.CO;2-E.
- [60] B.P. Rynne and P.D. Smith. Stability of time marching algorithms for the electric field integral equation. *J. Electromagn. Waves Appl.*, 4(12):1181–1205, 1990. doi: 10.1163/156939390X00762.
- [61] S. Sauter and A. Veit. A galerkin method for retarded boundary integral equations with smooth and compactly supported temporal basis functions. *Numer. Math.*, 123(1):145–176, 2013. doi: 10.1007/s00211-012-0483-7.
- [62] S. Sauter and A. Veit. Retarded boundary integral equations on the sphere: exact and numerical solution. *IMA J. Numer. Anal.*, 34(2):675–699, 2014. doi: 10.1093/imanum/drs059.
- [63] S. Sauter and A. Veit. Adaptive time discretization for retarded potentials. *Numer. Math.*, 132(3):569–595, 2016. doi: 10.1007/s00211-015-0726-5.
- [64] S.A. Sauter and C. Schwab. *Boundary Element Methods*, volume 39 of *Springer Series in Computational Mathematics*. Springer Berlin Heidelberg, 2011. doi: 10.1007/978-3-540-68093-2.

- [65] F.-J. Sayas. Energy estimates for galerkin semidiscretizations of time domain boundary integral equations. *Numer. Math.*, 124(1):121–149, 2013. doi: 10.1007/s00211-012-0506-4.
- [66] F.-J. Sayas. *Retarded Potentials and Time Domain Boundary Integral Equations: A Road Map*, volume 50 of *Springer Series in Computational Mathematics*. Springer, Cham, 2016. doi: 10.1007/978-3-319-26645-9.
- [67] R. Saye. High-order quadrature methods for implicitly defined surfaces and volumes in hyperrectangles. *SIAM J. Sci. Comput.*, 37(2):A993–A1019, 2015. doi: 10.1137/140966290.
- [68] M. Schanz. *Wave Propagation in Viscoelastic and Poroelastic Continua: A Boundary Element Approach*, volume 2 of *Lecture Notes in Applied and Computational Mechanics*. Springer-Verlag Berlin Heidelberg, 2001. doi: 10.1007/978-3-540-44575-3.
- [69] O. Steinbach. Space-time finite element methods for parabolic problems. *Comput. Methods Appl. Math.*, 15(4):551–566, 2015. doi: 10.1515/cmam-2015-0026.
- [70] E.P. Stephan, M. Maischak, and E. Ostermann. Transient boundary element method and numerical evaluation of retarded potentials. In M. Bubak, G.D. van Albada, J. Dongarra, and P.M.A. Sloot, editors, *Computational Science - ICCS 2008*, pages 321–330, Berlin, Heidelberg, 2008. Springer Berlin Heidelberg. ISBN 978-3-540-69387-1. doi: 10.1007/978-3-540-69387-1_35.
- [71] A. Veit, M. Merta, J. Zapletal, and D. Lukáš. Efficient solution of time-domain boundary integral equations arising in sound-hard scattering. *Internat. J. Numer. Methods Engrg.*, 107(5):430–449, 2016. doi: 10.1002/nme.5187.
- [72] K. Voronin, C.S. Lee, M. Neumüller, P. Sepulveda, and P.S. Vassilevski. Space-time discretizations using constrained first-order system least squares (cfosl). *J. Comput. Phys.*, 373:863–876, 2018. doi: 10.1016/j.jcp.2018.07.024.
- [73] L. Wang and P.-O. Persson. A high-order discontinuous galerkin method with unstructured space–time meshes for two-dimensional compressible flows on domains with large deformations. *Comput. & Fluids*, 118:53–68, 2015. ISSN 0045-7930. doi: 10.1016/j.compfluid.2015.05.026.
- [74] M. Zank and O. Steinbach. Adaptive space-time boundary element methods for the wave equation. *PAMM. Proc. Appl. Math. Mech.*, 16(1):777–778, 2016. doi: 10.1002/pamm.201610377.